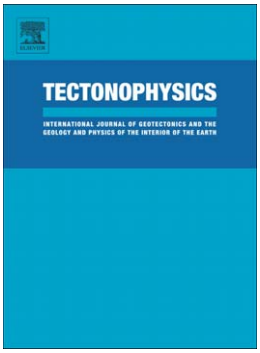

Relationships between very high pressure subduction complex assemblages and intrusive granitoids in the Tavşanlı Zone, Sivrihisar Massif, central Anatolia

Timothy A. Shin, Elizabeth J. Catlos, Lauren Jacob, Karen Black

PII: S0040-1951(12)00429-5
DOI: doi: 10.1016/j.tecto.2012.07.012
Reference: TECTO 125546

To appear in: *Tectonophysics*

Received date: 24 May 2011
Revised date: 11 May 2012
Accepted date: 21 July 2012

Please cite this article as: Shin, Timothy A., Catlos, Elizabeth J., Jacob, Lauren, Black, Karen, Relationships between very high pressure subduction complex assemblages and intrusive granitoids in the Tavşanlı Zone, Sivrihisar Massif, central Anatolia, *Tectonophysics* (2012), doi: 10.1016/j.tecto.2012.07.012

Relationships between very high pressure subduction complex assemblages and intrusive granitoids in the Tavşanlı Zone, Sivrihisar Massif, central Anatolia

Timothy A. Shin[a], Elizabeth J. Catlos[*,a], Lauren Jacob[b], Karen Black[a]

[a] University of Texas at Austin, Jackson School of Geosciences, Dept. Geological Sciences, 1 University Station C1100, Austin, 78712-0254, USA

[b] Apache Corporation, 2000 Post Oak Boulevard, Suite 100, Houston, Texas 77056-4400, USA

*=Corresponding author; telephone (+001-512-568-2183); fax (+001-512-471-5585); email (ejcatlos@gmail.com); address: University of Texas at Austin, Jackson School of Geosciences, Dept. Geological Sciences, 1 University Station C1100, Austin, 78712-0254, USA

Abstract. The Sivrihisar Massif of central Anatolia exposes blueschist and eclogite facies metasedimentary and metabasaltic rocks in close association with granitoid plutons. The massif is located within the Tavşanlı Zone, the subducted and exhumed northern continental margin of the Anatolide-Tauride Block. The relationship of the very high pressure assemblages to co-existing granitoid plutonic bodies (Kaymaz and Sivrihisar) is unclear as the region can be considered the type locality for the entrainment of excess argon in K-bearing minerals. Samples from its granitoids and a subduction complex assemblage were collected, imaged with cathodoluminescence (CL), and dated using zircon U-Pb *in situ* (in thin section) ion microprobe methods. The granitoids are heterogeneous as evidenced by CL images and geochemical variations. Finer-grained Sivrihisar samples are syenite and show plagioclase replacing K-feldspar, whereas coarser-grained rocks are monzonite and show the opposite reaction. Our samples of the Kaymaz granitoids are extremely Si rich (~82-97 wt% SiO_2) and have experienced sericitization. CL images of both granitoids show evidence for fluid interactions at both the subsolidus and lower temperature stages in their tectonic history. Subduction along the Tavşanlı Zone was ongoing during the Early to Late Cretaceous and entrained zircons with igneous zonation in CL that crystallized as early as the Paleoproterozoic. Sivrihisar Massif granitoids record zircon crystallization from the Late Cretaceous to Early Oligocene. Here we present a model in which the Sivrihisar and Kaymaz melts source from a subducting slab along the Afyon Zone further to the south and mix with an igneous component generated during decompression due to break off of the Tavşanlı slab. The model speculates that the Tavşanlı Zone is the northernmost segment of an amalgamation of stacked subduction zones that transition in activity from north to south over time.

Keywords. Sivrihisar Massif; Tavşanlı Zone; zircon geochronology; cathodoluminescence; slab break off; subduction

1. Introduction

Located in north central Turkey, the Tavşanlı Zone (Fig. 1) is one of the largest continuous expanses of exhumed subducted crust in the world (Okay, 1984, 1986, 2002; Davis and Whitney, 2006). Peak pressures up to ~26 kbar are recorded in Tavşanlı Zone blueschists and lawsonite-eclogites near the city of Sivrihisar (Davis and Whitney, 2006). These rocks provide a window into the exhumed northern continental margin of the Anatolide-Tauride Block affected by the closure of a branch of the Neo-Tethyan Ocean. The Sivrihisar Massif (Fig. 2) (Turkish for "pointed castle") is a portion of the Tavşanlı Zone that is comprised of a structurally coherent blueschist metamorphic belt containing hundreds of metabasalt pods that are, in places, intruded by granitoid plutons (Davis and Whitney, 2006; Whitney and Davis, 2006; Çetinkaplan et al., 2008; Whitney et al., 2011). Pressures observed in the lawsonite-eclogite in the portion of the exhumed subduction zone near Sivrihisar "… are among the highest reported for this rock type, which is rarely exposed at the Earth's surface" (Davis and Whitney, 2006). These very high pressure/low-temperature (HP/LT) rocks are within just a few kilometers of a pelitic assemblage containing coexisting aluminosilicate polymorphs (Whitney, 2002; Whitney et al., 2011). This relationship suggests significantly compressed isobars (~23 kbar/km) and the driving mechanism for this process is currently unknown.

Metamorphic belts such as the Tavşanlı Zone that consist of blueschist and eclogite rocks are commonly interpreted as remnants of subduction zones and occur globally. Such systems include the Franciscan Complex of California (e.g., Cloos, 1982), the Sanbagawa zone of Japan (e.g., Kabir and Takasu, 2010), and Alpine belts of Western Europe (e.g., Agard et al., 2009).

Commonly coupled with these metamorphic belts are granitoid arc-magma systems. For example, regions where granitoid bodies coexist next to or parallel to HP assemblages are portions of the Sierra Nevada (e.g., Saleeby et al., 2008), the Idaho Batholith (e.g., Manduca et al., 1993), Patagonia, Chile (e.g., Barbarin, 1999), and the Attic-Cycladic Crystalline Belt of the Aegean (e.g., Ring et al., 2010). In the Tavşanlı Zone, granitoids are intrusive to HP/LT footwall metamorphic rocks rather than parallel to them in the overriding hanging wall. Understanding this relationship is key for accurate reconstructions of the tectonic history of the Anatolide-Tauride Block.

Conflicting explanations for the tectonic relationship between the granitoid plutons and the Tavşanlı Zone exist (e.g., Harris et al., 1994; Delaloye and Bingöl, 2000; Whitney et al., 2011). This is likely due to the lack of age constraints on the timing between metamorphism and igneous intrusion. Tavşanlı Zone rocks commonly contain excess argon (Sherlock and Kelly, 2002), which has resulted in obscuring the age relationship between the granitoids and the metamorphic evolution of the Sivrihisar Massif. Here we review the current state of understanding of the tectonic history of the Tavşanlı Zone near Sivrihisar and provide new insight from major- and trace-element geochemistry, cathodoluminescence (CL) imagery, and *in situ* (in thin section) U-Pb ion microprobe zircon geochronology. The data are used to develop a model for development of the Sivrihisar Massif, a portion of the Tavşanlı Zone.

2. Geologic History

2.1. Overview

Turkey is an amalgamation of multiple crustal fragments due to the closure of several branches of Tethyan oceans and has as a result, a complex geology (Fig. 1) (Okay, 2008; Şengör and Atayman, 2009). Turkey largely formed in the Late Cretaceous as part of the orogeny that

resulted from collision between Laurasia and Gondwana (e.g., Şengör and Yılmaz, 1981; Okay, 1986). The country is commonly separated into four major tectonic divisions: the Pontides, Taurides, Anatolides, and Border Folds/Arabian Platform (Ketin, 1966; Şengör et al., 1980; Okay, 1984, 1986, 2008). This study focuses on the northernmost subdivision of the Anatolides (or Anatolian terrane), which is considered the strongly deformed equivalent of the Taurides. Many combine the two divisions into the Anatolide-Tauride Block (Figs. 1 and 3).

The Pontides are separated from the Taurides, Anatolides, and Border Folds by obducted ophiolites which partly comprise the Neo-Tethyan İzmir-Ankara-Erzincan Suture Zone (IAESZ). The Pontides have comparable units in the Balkans and Caucasus (Okay, 2008) and are considered a portion of Laurasia. The Taurides, Anatolides, and Border Folds/Arabian Platform are remnants of Gondwana to the south. The Sakarya Zone is a major part of the Pontides and predominantly consists of Precambrian to Paleozoic crystalline basement and late Triassic blueschists and eclogites covered by Jurassic to Eocene sediments. The Anatolides (Figs. 1 and 3) are subdivided into the Tavşanlı Zone, Afyon Zone, Menderes Massif, and Lycian Nappes (Okay 1984, 1986).

The Tavşanlı Zone is interpreted to represent the Mesozoic to Eocene closing of the northern branch of the ancient Neo-Tethyan Ocean between Laurasia, Gondwana, and associated microcontinents (e.g., Okay, 1984; Okay et al., 1998; Okay, 2008; Moix et al., 2008). The zone extends 250-350 km in length and is 40-100 km wide (Okay, 1984, 1986; Sherlock et al., 1999) and is largely composed of a coherent blueschist sequence overlain by a Cretaceous accretionary complex as a result of northward-dipping subduction. Portions of the Tavşanlı Zone are interpreted to have undergone Late Cretaceous subduction metamorphism (e.g., Sherlock et al., 1999; Whitney et al., 2011). Post-peak HP/LT metamorphism is considered to have occurred

~85-80 Ma based on Rb-Sr phengite ages that time crystallization during retrogression from peak metamorphic conditions (Sherlock et al., 1999). The unit experienced continental collision sometime in the Late Paleocene to Early Eocene (Okay, 1984, 1986; Sherlock et al., 1999). However, the timing of collision is debated and poorly constrained (Harris et al., 1994; Aldanmaz et al., 2006).

The Afyon Zone was previously interpreted as a greenschist facies passive margin sequence (Okay, 1984, 1986). However, the presence of Fe-Mg carpholite and glaucophane in metasediments and basement rocks, respectively, suggests it is an Alpine blueschist-facies metamorphic zone (Candan et al., 2005; Pourteau et al., 2010a). Metamorphism of the Afyon Zone may have occurred during the latest Cretaceous to early Cenozoic times (Candan et al., 2005; Okay, 2008; Pourteau et al., 2010a,b).

Tables 1-3 compile the existing mineral ages from metamorphic and igneous assemblages from the Tavşanlı Zone in general and the Sivrihisar Massif specifically. A transition from flysch to molasse sedimentation in the Sakarya Zone and the southward thrusting of peridotite over the Afyon zone indicate collision occurred sometime during the Paleocene (Okay et al., 1998). K-Ar and $^{40}Ar/^{39}Ar$ ages of minerals in both granitoid and metamorphic rocks from the Tavşanlı Zone are commonly affected by excess argon (Tables 1-3) (Cogulu and Krummenacher, 1967; Harris et al., 1994; Okay and Kelley, 1994; Sherlock et al., 1999; Sherlock and Arnaud, 1999; Sherlock and Kelley, 2002; Seaton et al. 2009).

2.2. Sivrihisar Massif

2.2.1 Metamorphic assemblages

The Sivrihisar Massif lies within the Eskişehir Fault Zone, a horst-graben series in the eastern portion of the Tavşanlı Zone (Fig. 2) (Özsayin and Dirik, 2007). The region has a

coherent basal unit termed the Orhaneli Unit (Fig. 3), which is composed of blueschist-facies metapelite overlain by marble that is up to several kms thick (Okay, 1984). The marble has been correlated to carbonates of the Anatolide-Tauride Block (Çetinkaplan et al., 2008) and may be in fault contact with the overlying lawsonite-bearing eclogite metabasite and metapelites (compare Okay, 1984 and Çetinkaplan et al., 2008).

The Ovacik Unit and an ophiolite peridotite slab overlies the Orhaneli Unit (Fig. 3). The Ovacik Unit represents a Cretaceous accretionary complex, and is comprised of imbricated, strongly tectonized serpentinites, pelagic shales, flow/sill basalts, pelagic limestones, and radiolarian cherts that underwent blueschist-facies metamorphism (Çetinkaplan et al., 2008). This unit is strongly sheared and lacks individual lithologies that can be traced more than a few hundred meters (Davis and Whitney, 2006). Lawsonite-eclogites in the unit are commonly observed as lozenge-shaped bodies that range up to 3 m thick and 10 m long (aligned parallel to foliation) (e.g., Whitney et al., 2011). These pods are commonly enclosed in an envelope of garnet-lawsonite glaucophanites. The eclogite-glaucophanite gradational contact is defined by increasing foliation intensity and replacement of omphacite by glaucophane. The eclogitic cores themselves are weakly foliated. Omphacite, lawsonite, and garnet have been observed in these rocks (Davis and Whitney, 2006; Whitney et al., 2011).

Peak pressures and temperatures of blueschist and lawsonite-eclogite pods of the Ovacik Unit are 24±2.5 kbar and 500±50°C and are thought to have formed prior to ~80 Ma (Sherlock and Kelley, 2002). Post-peak HP/LT metamorphism from Sivrihisar blueschist assemblages may be constrained by Rb-Sr phengite ages ranging from 82.8±1.7 Ma to 80.1±1.6 Ma (Sherlock et al., 1999). Phengite from these assemblages have $^{40}Ar/^{39}Ar$ ages that range from 168±49 Ma to 72±3 Ma (Table 2) (Sherlock et al, 1999; Sherlock and Kelley, 2002), likely due to the presence

of excess argon. $^{40}Ar/^{39}Ar$ muscovite ages of 60.4±0.1 Ma to 58.8±0.1 Ma may time the latest cooling during exhumation of the subduction zone (Seaton et al., 2009), but these ages may also be affected by excess argon. Davis and Whitney (2006) report temperatures as low as 380°C at ~12 kbar for the lawsonite-blueschist of Sivrihisar. The distinct pods in the Ovacik Unit are thought to be formed by imbrication and deformation during entrainment of blueschist- to eclogite-facies metamorphosed rock (e.g., Cloos, 1982; Davis, 2011).

A peridotite slab exists at the highest structural levels in the Sivrihisar region (Fig. 3) (e.g., Okay, 1984; Çetinkaplan et al., 2008). This unit may be metamorphosed due to movement along the IAESZ (Davis and Whiney, 2006), although elsewhere in the Tavşanlı zone, equivalent units may not have experienced blueschist-facies metamorphism (Okay and Kelley, 1994).

2.2.2 Igneous assemblages

The Sivrihisar and Kaymaz granitoid plutons (Fig. 4) were emplaced in a post-collisional (e.g., Harris et al. 1994; Whitney et al., 2011) or subduction zone setting (Delaloye and Bingöl, 2000; Kibici et al., 2008; Ilbeyli and Kibici, 2009), and may be part of a larger system, referred to as the Günyüzü pluton (Fig. 2) (Kibici et al., 2008; Ilbeyli and Kibici, 2009). The Sivrihisar and Kaymaz plutons are intrusive to both the Barrovian and HP/LT blueschist and eclogite metamorphic rocks in the region (e.g., Whitney et al., 2011), but only the Kaymaz granitoid is found in contact with the peridotite slab (Örgün et al., 2005).

The Sivrihisar pluton has been termed a granodiorite (Sherlock et al., 1999), alkali monzodiorite (Örgün et al., 2005) or monzonite (Delaloye and Bingöl, 2000) and has been reported to contain quartz, orthoclase, microcline, andesine, hornblende, biotite, and accessory and opaque minerals (sphene, zircon, apatite, magnetite, pyrite and chalcopyrite) (Örgün et al., 2005). See Table 4 for the mineral assemblages for the samples collected in this study. The

granitoid displays NW-SE trending emplacement cooling joints, is commonly intruded by aplite and pegmatitic dikes and contains sheared mafic enclaves (Fig. 4). The Kaymaz pluton is a sub-alkaline granitoid with a similar composition to the Sivirihisar granitoid, but also has been reported to contain oligoclase, allanite, tourmaline, and epidote (Örgün et al., 2005). We noted that the Kaymaz pluton is more weathered than the Sivrihisar exposures with K-feldspar often showing sericitization textures.

Table 3 reports ages of the Sivrihisar and Kaymaz granitoids, which range from 90.82±2.14 Ma (U-Pb zircon) to 48.95±4.49 Ma (U-Pb apatite; Gautier, 1984 referenced in: Delaloye and Bingöl, 2000; Whitney and Davis, 2006; Kibici et al., 2008). Due to the range, it is unclear if the plutons coincide with, post-date, or are completely unrelated to subduction during the Late to Early Cretaceous. A commonly cited age of the Sivrihisar granodiorite intrusion is 53±3 Ma (Sherlock et al., 1999) based on $^{40}Ar/^{39}Ar$ analyses of a hornblende clearly affected by excess argon (Fig. 5). The only reported age for the Kaymaz pluton is 84.98±6.27 Ma (U-Pb zircon; Gautier, 1984).

3. Materials and methods

Samples of the Sivrihisar (TA04, TA04A, TA04A-1, TA04A-2, TA04B) and Kaymaz plutons (TA05A, TA05B), mica schist (TA02A) were collected (Fig. 2; Table 4). Samples TA04, TA04A, and TA04A-2 are coarse-grained Sivrihisar granitoid assemblages, whereas TA04A-1 and TA04B are fine-grained (Fig. 6). The mica-schist sample is located in a region that has been mapped as part of a transition zone between Barrovian metamorphism and HP metamorphism (Whitney et al., 2011). Attempts were made to find reported localities of coexisting aluminosilicate-bearing rocks (Whitney, 2002) but were unsuccessful. Standard 20μm thin sections were made and polished for use in electron and ion beam machines. To locate zircons

suitable for geochronology, we employed scanning electron microscopy (SEM) with qualitative energy dispersive X-ray spectroscopy.

Two chips from Sivrihisar granitoid (fine-grained TA04A-1 and coarse-grained TA04A-2) and two samples from the Kaymaz granitoid (TA05A and TA05B) were sent to Activation Laboratories in Canada to obtain concentrations of major and trace elements (Fig. 7; Tables 5 and 6). All major elements and Sc, Be, V, Ba, Sr, Y, Zr were obtained using Fusion Inductively Coupled Plasma Spectrometry (ICP), whereas all other elements were detected using Fusion ICP/Mass Spectrometry.

Granitoid thin sections were texturally analyzed using cathodoluminescence (CL) at the Department of Mineralogical Sciences at the National Museum of Natural History at the Smithsonian Institution using a Premier American Technologies Luminoscope model ELM-3R (Fig. 6) (see methods outlined by Sorensen et al., 2006). Digital pictures were edited for brightness and contrast using image processing software. Dated zircons were also imaged using backscattered electrons (BSE) and CL using FEI Nova NanoSEM 430 with attached Gatan Chroma CL-SP detector at UT Austin's Bureau of Economic Geology (Figs. 8-10). The SEM-CL was operated in high vacuum mode with an accelerating voltage of 10 kV and ~1.3 nA current.

Zircon grains suitable for geochronology were sliced out of rock thin sections using a high-precision saw and mounted with a polished block of zircon standards (AS3, 1099±1 Ma; Schneider et al., 1999) after methods outlined in Catlos et al. (2002). Absolute U-Pb ages were determined from zircon grain in rock thin section using the non-destructive high-sensitivity/high-resolution Cameca IMS 1270 Ion Microprobe at UCLA (Table 7). In this method, a beam of primary ions bombards a zircon grain and erodes as little as ~10Å of the sample surface during a

typical 15 minute analysis. The UCLA SIMS operated with a mass resolution of 4800, a primary accelerating voltage of -12.5 kV, a secondary voltage of ~10 kV, an arc current ~74.7-74.9 mA, field aperture dimension 1500μm wide, and transfer lens settings that correspond to a field aperture/sample surface magnification factor of 100x. The ion microprobe zircon calibration curve had an equation of $UO^+/U^+ = 0.425$(Pb/U Relative Sensitivity Factor) + 5.811±0.152 for the AS3 standard. Because the primary beam spot size (~30μm) was at times larger than the dated zircon grains (Figs. 8-10), the aperture window and transfer lens settings were used to restrict contamination from regions outside the grain boundary. Thus, only small portions of the interior of the zircon grains were sampled. We apply two standard common Pb corrections and report the ages in Table 7.

4. Results

4.1. Thin section CL interpretations

Minerals that show colors in CL imagery in the Sivrihisar and Kaymaz granitoids are plagioclase (green), K-feldspar (blue, purple), calcite (orange), and apatite (yellow) (Fig. 6). Quartz, biotite, pyroxene, and muscovite in both rocks are dark gray to black.

Sample TA04 is a coarse-grained granitoid collected from the Sivrihisar pluton. This rock appears fresh in hand sample but shows ample evidence for fluid alteration and deformation in CL (Fig. 6). K-feldspar in the rock shows patchy blue zoning (Fig. 6B) (Parsons et al., 2008). The removal of blue luminescence in K-feldspar is thought to be driven by fluids (e.g., Finch and Klein, 1999). The core of a K-feldspar grain in this sample has a muscovite inclusion, also suggesting hydration during retrogression. Some plagioclase grains have brighter green cores and darker green rims, which can be related to differing amounts of calcium (Catlos et al., 2011). In sample TA04, plagioclase replaces K-feldspar through grain-boundary migration (Fig. 6B).

Pyroxene grains in the sample are weakly luminescent, but show a mottled, web-like texture, also due to alteration. We speculate that Ca-rich fluids may drive this alteration, as the pyroxene grains shows green veining. Sample TA04A shows similar CL properties as TA04, but we also observe plagioclase veins located within K-feldspar (Fig. 6C). These veins may have occurred during subsolidus deformation and are likely filling microcracks within the K-feldspar.

Sample TA04B is strikingly different than TA04 or TA04A, as in this rock as K-feldspar is being replaced by plagioclase (Fig. 6D). In Figure 6D, we speculate about possible options regarding boundaries of a plagioclase grain. As with sample TA04 and TA04A, this grain has a distinctly cracked core, a texture commonly observed in rocks that have experienced magma mixing (Tsuchiyama and Takahashi, 1983; Catlos et al., 2011). Sample TA04B differs in that it is finer-grained than TA04 or TA04A and contains K-feldspar grains with distinct purple cores and lighter blue rims.

Kaymaz sample TA05A is more weathered than the Sivrihisar samples (Fig. 6E) and shows the presence of significant fluid alteration with bright blue K-feldspar altering to clay. Calcite partially fills some microcracks, consistent with fluid-induced deformation. The rock contains many open microcracks that are blunted at the K-feldspar grain boundaries.

4.2. Geochemistry

Major- and trace- element analyses from the Sivrihisar and Kaymaz plutons (Tables 5 and 6) were plotted to distinguish chemical differences between the rocks (Fig. 7). Only two other studies report geochemistry of the Sivrihisar and Kaymaz plutons (Delaloye and Bingöl, 2000; Örgün et al., 2005) thus we also consider information from the potentially related Günyüzü plutonic suite (Fig. 2) (Kibici et al., 2008). The Sivrihisar and Kaymaz samples are high-K igneous rocks, and analyses from the Günyüzü pluton are consistent with predominantly

medium- and high-K affinities with one shoshonitic analysis. Samples from these plutons vary significantly in composition, showing a range between monzonite, syenite, and granite (senso stricto) on the total alkali discrimination diagram (Wilson, 1989) (Fig. 7A). The coarser-grained Sivrihisar sample (TA04A-2) is a monzonite, whereas the finer-grained sample (TA04A-1) is syenite. Örgün et al. (2005) report compositions from the Sivrihisar pluton between these end-members. Although the Kaymaz samples analyzed in this study are silica-rich (Table 5; Fig. 7A), higher Si contents from this pluton is not unusual (see Delaloye and Bingöl, 2000; Örgün et al., 2005). We speculate that sample TA05B (SiO_2 ~96.43 wt%; Table 5) lost its primary igneous character due to alteration also based on its low REE contents (e.g., Alderton et al. 1980).

In general, Sivrihisar granitoids are alkali-calcic and metaluminous whereas the Kaymaz rocks are more calcic and peraluminous (Table 5). With the exception of the extremely Si-rich Kaymaz sample TA05B, the Sivrihisar and Kaymaz pluton samples become more ferroan with increasing SiO_2 (wt%), following a trend outlined by the Günyüzü granitoids (Fig. 7B). All granitoids analyzed in the Sivrihisar Massif also decrease in $CaO + Al_2O_3$ with increasing silica contents (Fig. 7C), consistent with fractional crystallization of plagioclase or other minerals bearing these elements.

In terms of trace element diagrams, we found chondrite-normalized rare earth element (REE) diagrams show similar trends for the Sivrihisar samples, but Kaymaz rocks contain low amounts of REE (Table 6). Günyüzü granitoids are enriched in heavy REE and exhibit negative Zr anomalies compared to the other plutons. Primitive mantle-normalized trace element spider diagrams (Sun and McDonough, 1989) for Sivrihisar, Kaymaz, and Günyüzü plutons show the rocks have negative Nb, P, and Ti anomalies. Sivrihisar and Kaymaz granitoids exhibit positive anomalies in Pb. Sivrihisar, Kaymaz, and Günyüzü data in the Rb vs. (Y+Nb) tectonomagmatic

discrimination diagram (Pearce et al., 1984) (Fig. 7D) indicate the majority of the granitoids are consistent with a volcanic arc tectonic setting. One Kaymaz sample plots within the field of syn-collisional granitoids and one on the boundary of within-plate granitoids (Fig. 7D). However, use of the post-collisional field modification (Pearce, 1996) indicates many of the geochemical analyses share similar characteristics with other granitoids generated at this type of setting. The use of the post-collisional field demonstrates the chemical variability of these rocks, and we are unable to discriminate them from the other potential environments (Pearce, 1996). Plotting the data on other tectonomagmatic discrimination diagrams [major elements (Maniar and Piccoli, 1989); Rb vs. Y, vs. (Y+Ta), and vs. (Yb+Ta), Ta vs. Yb (Pearce et al., 1984), and ternary Hf-Rb-Nb and Hf-Rb-Ta diagrams (Harris et al., 1986)] was also of little use as these did not distinguish consistent sources for the same analyses. Overall, the major- and trace-element data suggest these granitoids have seen a complicated history; they may have been generated from subduction, and later mixed with syn-collisional and/or post-collisional melts derived from crustal sources. Their CL images are consistent with this interpretation (Fig. 6).

4.3. Geochronology

Because the CL images and geochemical data from these rocks show post-crystallization alteration, we targeted zircon for dating. The zoning of grains seen using CL and BSE provide information regarding their crystallization history (e.g., Hanchar and Miller, 1993). The colors of the dated zircon grains are yellow, black, blue, and/or green. The causes of CL intensities and the elements and/or factors that influence CL color and intensity of zircon in panchromatic SEM-CL images is debated and poorly understood (Nasdala et al., 2003; Gotze and Kempe, 2008). Blue and yellow CL emissions of zircon are attributed mainly to trace element Dy^{3+} contents, but Sm^{3+}, Y^{3+}, Eu^{2+}, and Tb^{3+} may also be activators (e.g., Marshall, 1988; Hanchar and Rudnick,

1995; Corfu et al., 2003). The presence of Y^{3+}, Ti^{4+}, and U^{4+} may cause lattice defects in zircon resulting in yellow and blue CL emission (Hanchar and Rudnick, 1995). Zircons may also emit lower CL intensities because of radiation damage (Poller et al., 2001; Corfu et al., 2003; Nasdala et al., 2003). The electronic structure, radiation damage, and thermal history of a zircon grain may affect CL emission so that a simple relationship between color and trace element content cannot be determined (Nasdala et al., 2003). For example, some zircons have been shown to display blue color in CL images, but do not emit a blue band CL emission within the visible light spectrum resulting in the inability to determine which trace element causes the blue color in the image (Gotze and Kempe, 2008). Although it is difficult to determine the exact cause of CL in zircon, color CL imaging is a useful tool to understand possible changes in magmatic conditions as the grains crystallized. Note that this is the first time that color CL images of zircon grains have been reported for these plutons.

Most of the ages we obtained are concordant depending on the common Pb correction that is applied (Fig. 11; Table 7). Major controls on the uncertainty in the ages include the reproducibility of the ion microprobe calibration curve, amount of measured common Pb, amount of detectable Pb in the sample, and the tectonomagmatic history of the grain. Aperture windows were applied to minimize common Pb contamination and analyze from small regions within the ion microprobe spot on individual grains. We speculate the greater uncertainty in $^{235}U/^{207}Pb$ ages compared to $^{238}U/^{206}Pb$ ages in some zircon grains are likely due to low amounts of measureable ^{207}Pb relative to ^{206}Pb in the sample. In Figures 8-11 and in the discussion below, we report what we deem are the most accurate $^{238}U/^{206}Pb$ ages from each zircon analyzed.

Zircon ages from the Sivrihisar pluton range from Late Cretaceous (78.4±8.5 Ma) to Middle Eocene (42.4±2.3 Ma), whereas zircon grains from the Kaymaz pluton are Middle

Eocene (42.5±2.2 Ma) to Early Oligocene (33.3±2.0 Ma) (Table 7; Figs. 8 and 9). Zircons from the mica-schist sample, mapped as part of the transition zone between Barrovian metamorphism near the Sivrihisar granitoid and HP metamorphism (Whitney et al., 2011), yield a large range of ages from Paleoproterozoic (1859±102 Ma) to Late Cretaceous (86.9±7.2 Ma) (Table 7; Fig. 10).

Many of the images of zircons from Sivrihisar and Kaymaz plutons show zoning typical of igneous crystallization (Figs. 8 and 9) (Corfu et al., 2003). The oldest Sivrihisar zircon grains are less distinctive due to their small size (Fig. 8). In general, Eocene grains show concentric zoning consistent with igneous crystallization and Kaymaz zircons are often sector zoned. Zircon 6 from Kaymaz sample TA05A (Fig. 8E) shows a bright ring in CL, indicative of resorption of the grain during magma heating or mixing. Bright rings or lobate transgressive zones may be indicative of fluid alteration of zircon (Harley et al., 2007), but are only likely to occur in high temperature fluid systems and are not observed in the dated granitoids. The range of ages obtained from these plutons is consistent with the types of zoning patterns seen in the CL images of the zircons. We saw no relationship between zircon color and age.

CL images of zircons from the TA02A transition-zone-HP/LT-metamorphic sample show a range of textures and are dominated by a blue color (Fig. 10). The Paleoproterozoic, Cambrian, and Carboniferous ages likely time igneous crystallization because they display oscillatory zoning in CL. The Early to Late Cretaceous zircon grains in this sample are amorphous in CL and may have formed during metamorphism.

5. Discussion

5.1. Interpretation of results

U-Pb zircon ages in sample TA02A are similar to Paleoproterozoic, Cambrian, and Carboniferous $^{207}Pb/^{206}Pb$ zircon ages from the Orhaneli region, and suggest the protolith of the

mica schists may have been sourced by the Variscan belt during the Triassic prior to the rifting of Laurasia and Gondwana (Okay et al., 2008). The oldest Cretaceous zircon age we report (116±8 Ma; Fig. 10B) is also consistent results from a number of $^{40}Ar/^{39}Ar$ ages from a variety of minerals from the region (Table 1) and suggests metamorphism may have occurred as early as the Aptian.

CL images, geochemical information, and U-Pb zircon ages from the Sivrihisar and Kaymaz plutons indicate these granitoids have a complex tectomagmatic history. Zircons from granitoids dated in this study range from as early as Late Cretaceous (78.4±8.5 Ma) to the Early Oligocene (33.3±2.0 Ma). Unpublished, but commonly cited U-Pb zircon ages, 90.82±2.14 Ma and 84.98±6.27 in Sivrihisar and Kaymaz plutons, respectively (Table 3; Gautier, 1984), are the only other known zircon ages for these rocks. Both granitoids contain zircons that are of Eocene age, suggesting they share a similar source. Both rocks show ample evidence for magma mixing in CL (Fig. 6), including different K-feldspar to plagioclase feldspar reactions in adjacent samples, corroded plagioclase cores, and a range of textures and differing geochemical signatures from single outcrops. In addition, the zircon ages from these rocks may be affected by fluids that were generated due to the injection of hot magma into a hydrous HP/LT metamorphic host that possibly dehydrated. However, we do observe a narrow distribution of contact metamorphism around the plutons. Older ages from Sivrihisar pluton are attributed to a long history of crystallization for the pluton or assimilated zircons from previously crystallized granitic basement, which could be part of the Sivrihisar pluton itself. The presence of Oligocene zircons in the Kaymaz pluton suggests the potential for a westward younging of magmatism, which may be due to the evolution of the spatial distribution of the source or the conduits that access it.

We speculate that these granitoids were initially metaluminous, magnesian, alkalic, volcanic-arc rocks derived from a subducting slab that became more peraluminous, ferroan, and calcic over time. Fractional crystallization occurred during maturation of their volcanic-arc source. These granitoids may have later mixed with syn-collisional and/or crustally derived melts (e.g., Barbarin, 1999). Crustally derived melts may have been sourced by adiabatic decompression melts from hot asthenosphere induced by slab break off that upwelled and underplated continental crust (e.g., von Blanckenburg and Davis, 1995; Davies and von Blanckenburg, 1995; Cloos et al., 2005). Syn- to post-collisional melts may have been mixed with subduction generated melts causing the geochemical fingerprints observed in whole-rock geochemistry. Conversely, if the granitoids are truly predominantly post-collisional, these types of granites have been attributed to the break-off of a subducting slab in regions including western Newfoundland (Whalen et al., 2006) and Central Anatolia (Pearce et al., 1990; Ilbeyli et al., 2004). The use of isotopic geochemistry is the next step in ascertaining the environment of these rocks (e.g., Ilbeyli et al., 2004; Whalen et al., 2006).

5.2. Tectonic model

The Sivrihisar and Kaymaz granitoids experienced crystallization dominantly during the Eocene, ~30 m.y. after Early to Late Cretaceous subduction zone metamorphism within the Tavşanlı Zone. The structural position and intrusive contact of the plutons within the HP/LT metamorphic portion of the subduction zone indicate these rocks do not represent the magmatic arc of the Tavşanlı Zone. Fig. 12 presents a model proposed to explain the presence of the granitoid arc in the Tavşanlı Zone and a mechanism for the rapid exhumation of the blueschist/eclogite metamorphic assemblages. This model is similar to polysubduction zone

models proposed for the Northern Andes (e.g., Ramos, 2009) and Arequipa-Antofalla terrane of the Andes (e.g., Ramos, 2008) but differs in dimensions.

In Fig. 12A, Neo-Tethyan ocean basins are separated by rifted continental crust. The Orhaneli Unit, comprised of metasedimentary rocks deposited on continental crust, began subducting during the Early to Late Cretaceous based on the metamorphic zircon ages reported here and previously published Rb-Sr ages (Sherlock et al., 1999). The subduction zone entrained Paleoproterozoic (1859±102 Ma to 1628±81 Ma) and Cambrian (562±32 Ma) to Carboniferous (307±16 Ma) detrital zircons shed from north or northwestern Variscan belt (Okay et al., 2008). Development of the IAESZ and HP/LT region of the Tavşanlı Zone by northward subduction of mafic crust under the Sakarya microcontinent occurred within the subduction shear channel (Fig. 12A). Exhumation of HP/LT rocks occurred concurrently with metamorphism due to channel back-flow in the subduction shear channel perhaps as described by Cloos (1982). Channel back-flow may also be the mechanism of formation of intensely foliated, folded, and sheared blueschist/eclogite pods (e.g., Davis, 2011).

The HP/LT zone depth is estimated to be 70-80 km for Sivrihisar Massif metabasites (e.g., Whitney et al., 2011), thus we speculate that the subducting oceanic lithosphere near the Sivrihisar Massif could have been 150-200 km wide from north to south. Subduction could have occurred slowly (10-50 km/my) before negatively buoyant lithosphere was consumed. The magmatic arc related to the Tavşanlı Zone has not yet been found, interpreted as such, or never existed because subducted lithosphere never reached depths at which arc magmas are generated. The Tavşanlı Zone may represent flat and shallow subduction, preventing a typical magmatic/volcanic arc from forming northward of the margin. However, this idea has been disregarded by seismic tomographic studies (Dilek and Sandvol, 2009).

Fig. 12B provides a snapshot at ~85 Ma where exhumation of the Tavşanlı Zone continues at peak metamorphism and is concurrent with the initiation of northward Afyon Zone subduction to the south. The HP/LT Afyon Zone can be constrained by structural position to the latest Cretaceous to Early Cenozoic (Candan et al., 2005; Okay, 2008; Pourteau et al., 2010a,b) and is thrust under the Tavşanlı Zone (see also Delaloye and Bingöl, 2000), recording the closure of a southern branch of the Neo-Tethyan Ocean. Alternatively, the Tavşanlı and Afyon Zones may be stacks of HP/LT nappes (Pourteau et al., 2010a) rather than separate oceanic slabs that underwent subduction at different times (Fig. 12B). Although this scenario explains the presence of two HP/LT metamorphic belts and their apparent thrust contact, smaller scale nappe stacking does not explain granitoid intrusion into the HP/LT regions found within the Sivrihisar Massif.

In our model, Afyon Zone lithosphere subducts to depths that initiate slab dehydration, and the subsequent fluid flux generates granitoid magmas that crystallize between the Late Cretaceous to the Eocene (Fig. 12C). Magmas from the subducting lithosphere of the Afyon Zone intrude older metasomatized Tavşanlı HP/LT zone rocks. During this time, the Tavşanlı margin transitions to collision, which we define as the convergence of two plates when lithosphere can no longer subduct due to a lack of significant density differences. The new collisional setting in the Tavşanlı Zone develops as evidenced by the structural stacking of lithostratigraphic units (e.g., Çetinkaplan et al., 2008; Whitney et al., 2011).

The Tavşanlı Zone slab also breaks off in this timeframe, giving rise to magma mixing of (1) decompression melts that underplate a metasomatized and hydrated layer, (2) syn- to post-collisional granitoids, and (3) Afyon Zone subduction zone-generated melts. Slab break off allows for hot asthenosphere to undergo adiabatic decompression melting or be juxtaposed against thickened metasomatized and hydrated mantle lithosphere and cause syn-collisional

magmatism by underplating or conductive heating (e.g., Cloos et al., 2005). This would result in a linear east-west belt or belts of voluminous Cenozoic volcanism and plutonism as is seen in western and central Turkey (e.g., Harris et al., 1994; Aldanmaz et al., 2000; Delaloye and Bingöl, 2000; Akay and Erdogan, 2004; Aldanmaz et al., 2006; Okay and Satir, 2006; Altunkaynak, 2007; Karacık et al., 2007; Dilek and Altunkaynak, 2007, 2009). These magmatic belts are commonly attributed primarily to slab break off and lithospheric delamination (e.g., Dilek and Sandvol, 2009).

We speculate that exhumation of the Tavşanlı HP/LT zone likely increased during this time due to the presence of the Afyon subduction zone, tectonic shearing as the Tavşanlı crust transitioned from subduction to collision, channel back-flow processes operating within the Tavşanlı Zone subduction channel, and erosion. Intruding magmas may experience subsolidus deformation as observed in their textures (Fig. 6).

This process may have been repeated by the subduction of the Hellenic arc (Fig. 12D), which generated granitoids in the Menderes Massif and elsewhere in the Aegean (e.g., Delaloye and Bingöl, 2000). In Fig. 12D, we provide a snapshot of the system at ~30 Ma, where subduction and roll-back of the present day Hellenic Arc works to exhume the Menderes Massif metamorphic core complex. The Hellenic Arc forms a third subduction zone, comprised of the northward down-going oceanic lithosphere of the African Plate overridden by the Afyon Zone. This process may have also facilitated the transition from subduction to collision of the Tavşanlı Zone, which was largely completed by the Oligocene.

An alternative explanation of the arc-magma relationship within the Tavşanlı Zone would rely fully on slab break off for intra-subduction zone arc magmagenesis (e.g., Ramos, 2008). This model similarly initiates subduction of a 100 to 250 km-wide region of oceanic lithosphere

that contains portions of continental lithosphere. The subducting oceanic lithosphere again fails to achieve depths sufficient to generate a magmatic arc. By the Late Cretaceous, subduction in Tavşanlı Zone transitions to collision when all of the negatively buoyant lithosphere (oceanic) subducts, leaving only the positively buoyant lithosphere (continental) to collide with the Sakarya microcontinent. In this scenario, the negatively buoyant lithosphere separates from the positively buoyant lithosphere, causing the break off of the subducting Tavşanlı Zone slab (e.g., Cloos et al., 2005). Magmas produced would likely be initially potassic and calc-alkaline and shallower crustal melts would be granitic/rhyolitic (e.g., Dilek and Sandvol, 2009). Slab break off may have initiated in the east as indicated by zircon ages from the Sivrihisar and Kaymaz granitoids and from the Beypazari granite, located ~70 km north of the Sivrihisar Massif (Catlos et al., 2012). The initial zone of magmatism may be near the Central Anatolian Crystalline Complex, as unzipping westward hot asthenosphere upwells. The Afyon Zone could have experienced a similar slab break off event and its lack of typical magmatic arc also due to the small width of the subducting oceanic lithosphere. However, this model is less favorable than the polysubduction model because of the protracted tectonomagmatic history demonstrated by zircon ages, contrasting with the brevity of magmatism commonly associated with slab break off only (e.g., Whalen et al, 2006).

Recent teleseismic Pn velocity, Sn attenuation, and P-wave travel time tomography models (Dilek and Sandvol, 2009; Biryol et al., 2011) reveal segmented fast velocity seismic anomalies and slow velocity perturbations beneath the Sivrihisar Massif. Fast anomalies at deep depths (~400 km) beneath the Sakarya, Tavşanlı, and Afyon Zones are attributed to subducted slabs of the Cyprean and Hellenic arcs (Dilek and Sandvol, 2009; Biryol et al., 2011), whereas slow perturbations from 0 – 600 km depth are due to upwelling asthenosphere due to slab tear.

Fast seismic anomalies below the 660 km discontinuity beneath the Cyprean and Hellenic arcs may represent old detached remnant slab(s) (Dilek and Sandvol, 2009). Heterogeneities in the shape of the fast anomalies indicate the possibility of multiple detached or delaminated lithospheric fragments (Dilek and Sandvol, 2009), consistent with the model in Fig. 12. If a small (100-200 km wide) Tavşanlı Zone slab were to have broken off followed by one from the Afyon Zone (Fig. 12), they would likely appear as the thick fast seismic anomalies as seen in tomographic studies of the region.

Acknowledgements

This work was supported by the National Science Foundation (NSF) International Research Experiences for Students Award (#0937254), an Undergraduate Research Fellowship from UT Austin's University Co-operative Society, the Jackson School of Geosciences Undergraduate Honors Research Program, and the UT Austin's Department of Geological Sciences. Samples were obtained with the help of Middle East Technical University students Gökhan Okan Yıldız, Nilay Yağcıoğlu, and Sükrü Gökhan Köse (Dept. of Geological Engineering) and Oklahoma State University student Jessica Magers (Boone Pickens School of Geology). Thorough and constructive reviews and comments from Drs. Dimitrios Papanikolaou, Mark Cloos and Mark Helper, and three anonymous reviewers greatly improved the original manuscript. The authors thank the UCLA National Ion Microprobe Facility (particularly Drs. Axel Schmitt and Rita Economos), which is partially supported by funding from NSF's Instrumentation and Facilities Program. Ages were obtained with the help of Jackson School of Geosciences students Kathryn Huber and Heather Flynn. Thin-section scale CL imagery was generated with the support of the Smithsonian Institution's National Museum of Natural History Fellowship program awarded to Lauren Jacob under the supervision of Dr. Sorena Sorensen. We appreciated technical support

from Drs. Xiaohu Tang (UT Austin's Bureau of Economic Geology), Donggao Zhao (Jackson School of Geosciences). Figures were drafted with the assistance of Jackson School undergraduates Tyson McKinney and Pamela Speciale.

Figure Captions

Fig. 1. Tectonic map of the northeastern Mediterranean region (after Okay, 2008). Sutures are represented by heavy lines with small filled triangles (inactive subduction zones) and large open triangles (active subduction zones). Smaller open triangles represent polarity of fold and thrust belts. Box on the figure indicates the study area shown in Fig. 2.

Fig. 2. Simplified geologic map of the study area overlain on a hillshade raster. Map after Senel and Aydal (2002), Özsayin and Dirik (2007), and our observations.

Fig. 3. North-south cross section across western Turkey after Okay (1986). IAESZ= İzmir-Ankara-Erzincan Suture Zone.

Fig. 4. (A) Sivrihisar pluton. (B) Kaymaz pluton, relief is approximately 100 meters. (C) Aplite dike within the Sivrihisar granitoid at the same location as sample TA04. (D) Sheared mafic enclave in the Sivrihisar granitoid at the same location.

Fig. 5. (A) $^{40}Ar/^{39}Ar$ data from an infrared laser step-heated amphibole aliquot from Sivrihisar after Sherlock et al. (1999). (B) Inverse isochron (correlation diagram) of the same amphibole aliquot as (A) using data reported by Sherlock et al. (1999). Atmospheric argon is indicated for reference. The isochron plot shows this sample fails to show simple mixing between atmospheric argon and a trapped radiogenic component.

Fig. 6. (A) Hand samples of Sivrishar samples TA04, TA04A, TA04B, and Kaymaz sample TA05A. CL images of (B) Sivrihisar granitoid sample TA04, (C) TA04A, (D) TA04B, and (E) Kaymaz granitoid sample TA05A. Mineral abbreviations after Siivola and

Schmid (2007). Veins are indicated in panel (C). We speculate about possible options regarding boundaries of a plagioclase grain in panel (D).

Fig. 7. (A) Na_2O+K_2O versus SiO_2 diagram (Wilson, 1989) for Sivrihisar, Kaymaz, and Günyüzü plutons. Data are from our samples, Delaloye and Bingöl (2000), Kibici et al. (2008). A range of analytical information for the Sivrihisar pluton is indicated by a boxed "S" and from the Kaymaz pluton is a boxed "K" (from Örgün et al., 2005). Some samples are identified. (B) $Fe_2O_3/(Fe_2O_3 + MgO)$ and (C) $CaO + Al_2O3$ (wt%) vs. SiO_2 for the Sivrihisar, Kaymaz, and Günyüzü plutons. (D) Rb vs. (Y+Nb) discrimination diagram for the Sivrihisar, Kaymaz and Günyüzü plutons showing the syn-collisional (syn-COLG), within-plate (WPG), volcanic-arc (VAG), and ocean ridge (ORG) fields after Pearce et al. (1984). The post-collisional (post-COLG) field modification is also indicated (Pearce, 1996).

Fig. 8. CL (left) and BSE images (right) of zircon grains from Sivirhisar pluton sample TA04 (panels A-E) and TA04B (panel F). Grain numbers and ^{238}U-^{206}Pb ages (±1σ) are indicated above the images (see Table 7). Grains are outlined in the CL images and dashed lines indicate the location and size of the ion microprobe spot.

Fig. 9. CL (left) and BSE images (right) of zircon grains from Kaymaz pluton sample TA05A. Grain numbers and ^{238}U-^{206}Pb age (±1σ) are indicated above the images (see Table 7). Grains are outlined in the CL images and dashed lines indicate the location and size of the ion microprobe spot.

Fig. 10. CL (left) and BSE images (right) of zircon grains from mica schist sample TA02A. Grain numbers and ^{238}U-^{206}Pb age (±1σ) are indicated above the images (see Table 7).

Grains are outlined in the CL images and dashed lines indicate the location and size of the ion microprobe spot.

Fig. 11. U-Pb concordia diagrams of *in situ* ion microprobe analyses of zircons from (A) Sivrihisar pluton samples TA04 and TA04B. (B) Kaymaz pluton sample TA05A, and (C) mica schist sample TA02A.

Fig. 12. Lithospheric-scale cross sections of a model that describes intrusion of subduction generated metamorphic rocks by magmas sourced from progressively younger subduction zones. The subduction zone cartoon is adapted from Cloos et al. (2005). Overthrusting of km-scale slabs is not shown. Scale is only a rough approximation. (A) During the Early to Late Cretaceous, the Tavşanlı Zone develops. (B) At ~85 Ma peak metamorphism of Tavşanlı Zone occurs and the Afyon Zone develops due to subduction. (C) At ~45 Ma, granitoid arc magmas from the Afyon Zone intrude the Tavşanlı Zone. (D) At ~30 Ma Tavşanlı Zone slab break off allows adiabatic decompression melting in Tavşanlı lithospheric mantle. The Hellenic Arc experiences ongoing subduction. See text for further discussion.

References

Agard, P., Yamato, P., Jolivet, L., Burov, E., 2009. Exhumation of oceanic blueschists and eclogites in subduction zones: timing and mechanisms. Earth-Science Reviews 92, 53-79.

Akay, E., Erdoğan, B., 2004. Evolution of Neogene calc-alkaline to alkaline volcanism in the Aliağa-Foça region (Western Anatolia, Turkey). Journal of Asian Earth Sciences 24, 367-387.

Aldanmaz, E., Köprübaşı, N., Gürer, Ö.F., Kaymakçı, N., Gourgaud, A., 2006. Geochemical constraints on the Cenozoic, OIB-type alkaline volcanic rocks of NW Turkey: Implications for mantle sources and melting processes. Lithos 86, 50-76.

Aldanmaz, E., Pearce, J., Thirlwall, M., Mitchell, J., 2000. Petrogenetic evolution of late Cenozoic, post-collision volcanism in western Anatolia, Turkey. Journal of Volcanology and Geothermal Research 102, 67-95.

Alderton, D.H.M., Pearce, J.A., Potts, P.J., 1980. Rare earth element mobility during granite alteration: Evidence from southwest England. Earth and Planetary Science Letters 49, 149-165.

Altunkaynak, Ş., 2007. Collision-driven slab breakoff magmatism in Northwestern Anatolia, Turkey. Journal of Geology 115, 63-82.

Barbarin, B., 1999. A review of the relationships between granitoid types, their origins and their geodynamic environments. Lithos 46, 605-626.

Biryol, C.B., Beck, S.L., Zandt, G., Özacar, A.A., 2011. Segmented African lithosphere beneath the Anatolian region inferred from teleseismic P-wave tomography. Geophysical Journal International 184, 1037-1057.

Candan, O., Çetinkaplan**,** M., Oberhänsli**,** R., Rimmelé, G., Akal, C. **(**2005) Alpine high-P/low-T metamorphism of the Afyon Zone and implications for the metamorphic evolution of Western Anatolia, Turkey. Lithos, 84, 102-124.

Catlos, E.J., Baker, C.B., Sorensen, S.S., Jacob, L., Çemen, I., 2011. Linking microcracks and mineral zoning of detachment-exhumed granites to their tectonomagmatic history: Evidence from the Salihli and Turgutlu plutons in western Turkey (Menderes Massif). Journal of Structural Geology 33, 951-969.

Catlos, E.J., Gilley, L.D., Harrison, T.M., 2002. Interpretation of monazite ages obtained via in situ analysis. Chemical Geology 188, 193-215.

Catlos, E.J., Shin, T.A., Speciale, P., Yildiz, G.O., Black, K., 2012. Linked magmatic events in central Turkey: geochemistry and geochronology of the Beypazari and Sivrihisar granitoids. European Geosciences Union General Assembly 2012, Geophysical Research Abstracts 14, EGU2012-2497.

Çetinkaplan, M., Candan, O., Oberhänsli, R., Bousquet, R., 2008. Pressure-temperature evolution of lawsonite eclogite in Sivrihisar; Tavşanlı Zone-Turkey. Lithos 104, 12-32.

Cloos, M., 1982. Flow melanges: Numerical modeling and geologic constraints on their origin in the Franciscan subduction complex, California. Geological Society of America Bulletin 93, 330-334.

Cloos, M., Sapiie, B., van Ufford, A.Q., Weiland, R.J., Warren, P.Q., McMahon, T.P., 2005. Collisional delamination in New Guinea: The geotectonics of subducting slab breakoff. Geological Society of America Special Paper 400, pp. 1-51.

Cogulu, E., Krummenacher, D., 1967. Problemes geochronometricques dans la partie NW de l'Anatolie Centrale (Turquie). Schweizerische Mineralogische und Petrographische Mitteilungen 47, 825-833.

Corfu, F., Hanchar, J.M., Hoskin, P.W., Kinny, P., 2003. Atlas of zircon textures. Reviews in Mineralogy and Geochemistry 53, 469-500.

Davies, J.H., von Blanckenburg, F., 1995. Slab breakoff: A model of lithosphere detachment and its test in the magmatism and deformation of collisional orogens. Earth and Planetary Science Letters 129, 85-102.

Davis, P.B., 2011. Petrotectonics of lawsonite eclogite exhumation: Insights from the Sivrihisar massif, Turkey. Tectonics 30, TC1006. doi:10.1029/2010TC002713.

Davis, P.B., Whitney, D.L., 2006. Petrogenesis of lawsonite and epidote eclogite and blueschist, Sivrihisar Massif, Turkey. Journal of Metamorphic Geology 24, 823-849.

Delaloye, M., Bingöl, E., 2000. Granitoids from western and northwestern Anatolia: Geochemistry and modeling of geodynamic evolution. International Geology Review 42, 241-268.

Dilek, Y., Altunkaynak, Ş., 2007. Cenozoic crustal evolution and Mantle Dynamics of Post-Collisional Magmatism in Western Anatolia. International Geology Review 49, 431-453.

Dilek, Y., Altunkaynak, Ş., 2009. Geochemical and temporal evolution of Cenozoic magmatism in western Turkey: mantle response to collision, slab break-off, and lithospheric tearing in an orogenic belt. In: van Hinsbergen, D.J., Edwards, M.A., Grovers, R. (Eds.), Collision and collapse at the Africa-Arabia-Eurasia subduction zone: Geological Society London Special Publications, 311, pp. 213-233.

Dilek, Y., Sandvol, E., 2009. Seismic structure, crustal architecture and tectonic evolution of the Anatolian-African plate boundary and the Cenozoic orogenic belts in the Eastern Mediterranean Region. In: Murphy, J.B., Keppie, J.D., Hynes, A.J. (Eds.), Ancient orogens and modern analogs: Geological Society London Special Publications, 327, pp. 127-160.

Finch, A.A., Klein, J., 1999. The causes and petrological significance of cathodoluminescence emissions from alkali feldspars. Contributions to Mineralogy and Petrology 135, 234-43.

Frost, B.R., Barnes, C.G., Collins, W.J., Arculus, R.J., Ellis, D.J., Frost, C.D., 2001. A geochemical classification for granitic rocks. Journal of Petrology 42, 2033-2048.

Gautier, Y., 1984. Déformations et métamorphismes associés à la fermeture téthysienne en Anatolie centrale (région de Sivrihisar, Turquie). PhD thesis, University Paris-Sud, France. 236.

Gotze, J., Kempe, U., 2008. A comparison of optical microscope-and scanning electron microscope-based cathodoluminescence (CL) imaging and spectroscopy applied to geosciences. Mineralogical Magazine 72, 909-924.

Hanchar, J.M., Miller, C.F., 1993. Zircon zonation patterns as revealed by cathodoluminescence and backscattered electron images: Implications for interpretation of complex crustal histories. Chemical Geology 110, 1-13.

Hanchar, J., Rudnick, R., 1995. Revealing hidden structures: The application of cathodoluminescence and back-scattered electron imaging to dating zircons from lower crustal xenoliths. Lithos 36, 289-303.

Harley, S.L., Kelly, N.M., Möller, A., 2007. Zircon behaviour and the thermal histories of mountain chains. Elements 3, 25-30.

Harris, N.B.W., Kelley, S., Okay, A.I., 1994. Post-collision magmatism and tectonics in northwest Anatolia. Contributions to Mineralogy and Petrology 117, 241-252.

Harris, N.B.W., Pearce, J.A., Tindle, A.G., 1986. Geochemical characteristics of collision-zone magmatism. In: Coward, M.P., Ries, A.C. (Eds.), Collision tectonics: Geological Society London Special Publications, 19, pp. 67-81.

Ilbeyli, N., Kibici, Y., 2009. Collision-related granite magma genesis, potential sources and tectono-magmatic evolution: comparison between central, northwestern and western Anatolia (Turkey). International Geology Review 51, 252-278.

Ilbeyli, N., Pearce, J.A., Thirlwall, M.F., Mitchell, J.G., 2004. Petrogenesis of collision-related plutonics in Central Anatolia, Turkey. Lithos 72, 163-182.

Kabir, M.F., Takasu, A., 2010. Evidence for multiple burial-partial exhumation cycles from the Onodani eclogites in the Sambagawa metamorphic belt, central Shikoku, Japan. Journal of Metamorphic Geology 28, 873-893.

Karacık, Z., Yılmaz, Y., Pearce, J.A., Ece, Ö.I., 2007. Petrochemistry of the south Marmara granitoids, northwest Anatolia, Turkey. International Journal of Earth Sciences 97, 1181-1200.

Ketin, I., 1966. Tectonic units of Anatolia. *Bulletin of the Mineral Research* and *Exploration of Turkey* 66, 23-24.

Kibici, Y., Ilbeyli, N., Yildiz, A., Bagci, M., 2008. Geochemical constraints on the genesis of the Günyüzü Pluton, Northwest Anatolia, Turkey. International Geology Review 50, 931-947.

Manduca, C.A., Kuntz, M.A., Silver, L.T, 1993. Emplacement and deformation history of the western margin of the Idaho Batholith near McCall, Idaho; influence of a major terrane boundary. Geological Society of America Bulletin 105, 749-765.

Maniar, P.D., Piccoli, P.M., 1989. Tectonic discrimination of granitoids. Geological Society of America Bulletin 101, 635-643.

Marshall, D.J., 1988. Cathodoluminescence of geological materials. Unwin Hyman, Boston.

Moix, P., Beccaletto, L., Kozur, H.W., Hochard, C., Rosselet, F., Stampfli, G.M., 2008. A new classification of the Turkish terranes and sutures and its implication for the paleotectonic history of the region. Tectonophysics 451, 7-39.

Nasdala, L., Zhang, M., Kempe, U., Panczer, G., Gaft, M., Andrut, M., Plotze, M. 2003. Spectroscopic methods applied to zircon. Reviews in Mineralogy and Geochemistry 53, 427-467.

Okay, A.I., 1984. Distribution and characteristics of the north-west Turkish blueschists. In: J.E. Dixon, J.E., Robertson, A.H.F. (Eds.), The geological evolution of the Eastern Mediterranean: Geological Society London Special Publications, 17, pp. 455-466.

Okay, A. I., 1986. High-pressure/low-temperature metamorphic rocks of Turkey. In: Evans, B.W., Brown, E.H. (Eds.), Blueschists and eclogites. Memoir-Geological Society of America, 164, pp. 333-347.

Okay, A.I., 2002. Jadeite-chloritoid-glaucophane-lawsonite blueschists in north-west Turkey: unusually high P/T ratios in continental crust. Journal of Metamorphic Geology 20, 757-768.

Okay, A.I., 2008. Geology of Turkey: A synopsis. Anschnitt 21, 19-42.

Okay, A.I., Harris, N.B.W., Kelley, S.P., 1998. Exhumation of blueschists along a Tethyan suture in northwest Turkey. Tectonophysics 285, 275-299.

Okay, A.I., Kelley, S.P., 1994. Tectonic setting, petrology and geochronology of jadeite + glaucophane and chloritoid + glaucophane schists from north-west Turkey. Journal of Metamorphic Geology 12, 455-466.

Okay, A.I., Satır, M., 2006. Geochronology of Eocene plutonism and metamorphism in northwest Turkey: evidence for a possible magmatic arc. Geodinamica Acta 19, 251-266.

Okay, A.I., Satır, M., Shang, C.K., 2008. Ordovician metagranitoid from the Anatolide-Tauride Block, northwest Turkey: geodynamic implications. Terra Nova 20, 280-288.

Örgün, Y., Altinsoy, N., Gültekin, A.H., Karahan, G., Çelebi, N., 2005. Natural radioactivity levels in granitic plutons and groundwaters in Southeast part of Eskisehir, Turkey. Applied Radiation and Isotopes 63, 267-275.

Özsayin, E., Dirik, K., 2007. Quaternary Activity of the Cihanbeyli and Yeniceoba Fault Zones: İnönü-Eskişehir Fault System, Central Anatolia. Turkish Journal of Earth Science 16, 471-492.

Parsons, I., Steele, D.A., Lee, M.R., Magee, C.W., 2008. Titanium as a cathodoluminescence activator in alkali feldspars. American Mineralogist 93, 875 -879.

Pearce, J., 1996. Sources and settings of granitic rocks. Episodes 19, 120-125.

Pearce, J.A., Bender, J.F., Long, S.E.D., Kidd, W.S.F., Low, P.J., Güner, Y., Saroglu, F., Yilmaz, Y., Moorbath, S., Mitchell, J.G., 1990. Genesis of collision volcanism in Eastern Anatolia, Turkey. Journal of Volcanology and Geothermal Research 44, 189-229.

Pearce, J.A., Harris, N.B.W., Tindle, A.G., 1984. Trace element discrimination diagrams for the tectonic interpretation of granitic rocks. Journal of Petrology 25, 956-983.

Poller, U., Hugh, J., Hoppe, P., and Williams, I.S. 2001. REE, U, Th, and Hf distribution in zircon from western Carpathian Variscan granitoids: a combined cathodoluminescence and ion microprobe study. American Journal of Science 301, 858-876.

Pourteau, A., Candan, O., Oberhänsli, R., 2010a. High-pressure metasediments in central Turkey: Constraints on the Neotethyan closure history. Tectonics 29, 1-18.

Pourteau, A., Candan, O., Oberhänsli, R., Sudo, M., 2010b. $^{40}Ar/^{39}Ar$ dating of subduction-related metamorphism in the Anatolide HP belt, W-Turkey: Implications for the evolution of the Eastern Mediterranean. European Geosciences Union General Assembly 2010, Geophysical Research Abstracts 12, EGU2010-3996.

Ramos, V.A., 2008. The basement of the Central Andes: The Arequipa and related terranes. Annual Review of Earth and Planetary Sciences 36, 289-324.

Ramos, V.A., 2009. Anatomy and global context of the Andes: Main geologic features and the Andean orogenic cycle. In: Kay, S., Ramos, V., Dickinson, W. (Eds.), Backbone of the Americas: Shallow subduction, plateau uplift, and ridge and terrane collision: Memoir-Geological Society of America, 204, pp. 31-65.

Ring, U., Glodny, J., Will, T., Thomson, S., 2010. The Hellenic subduction system: High-pressure metamorphism, exhumation, normal faulting, and large-scale extension. Annual Review of Earth and Planetary Sciences 38, 45-76.

Saleeby, J.B., Ducea, M.N., Busby, C.J., Nadin, E.S., Wetmore, P.H. 2008. Chronology of pluton emplacement and regional deformation in the southern Sierra Nevada Batholith, California. In: Wright, J.E., Shervais, J.W. (Eds.), Ophiolites, arcs, and batholiths; a tribute to Cliff Hopson. Geological Society of America Special Paper, 438, pp. 397-427.

Schneider, D., Edwards, M., Kidd, W.S., Zeitler, P., Coath, C., 1999. Early Miocene anatexis identified in the western syntaxis, Pakistan Himalaya. Earth and Planetary Science Letters 167, 121-129.

Seaton, N.C.A., Whitney, D.L., Teyssier, C., Toraman, E., Heizler, M.T., 2009. Recrystallization of high-pressure marble (Sivrihisar, Turkey). Tectonophysics 479, 241-253.

Senel, M., Aydal, N., 2002, Geological Map of Turkey (Ankara sheet), Maden Tetkik ve Arama Genel Mudurlugu, Eskisehir Yolu, Turkey.

Şengör, A.M.C., Atayman, S., 2009. The Permian Extinction and the Tethys: An Exercise in Global Geology. Geological Society of America Special Paper, 448, pp. 1-85.

Şengör, A.M.C., Yilmaz, Y., 1981. Tethyan evolution of Turkey: A plate tectonic approach. Tectonophysics 75, 181-241.

Şengör, A.M.C., Yilmaz, Y., Ketin, İ., 1980. Remnants of a pre-Late Jurassic ocean in northern Turkey: Fragments of Permian-Triassic Paleo-Tethys? Geological Society of America Bulletin 91, 599-609.

Sherlock, S., Arnaud, N.O., 1999. Flat plateau and impossible isochrones: Apparent ^{40}Ar-^{39}Ar geochronology in a high pressure terrane. Geochimica et Cosmochimica Acta 63, 2835-2838.

Sherlock, S., Kelley, S., 2002. Excess argon evolution in HP-LT rocks: a UVLAMP study of phengite and K-free minerals, NW Turkey. Chemical Geology 182, 619-636.

Sherlock, S., Kelley, S., Inger, S., Harris, N., Okay, A., 1999. ^{40}Ar-^{39}Ar and Rb-Sr geochronology of high-pressure metamorphism and exhumation history of the Tavsanli Zone, NW Turkey. Contributions to Mineralogy and Petrology 137, 46-58.

Siivola, J., Schmid, R., 2007. Classification and nomenclature scheme; list of mineral abbreviations. In Fettes, D., Desmons, J., (Eds.) Metamorphic rocks, a classification and glossary of terms; recommendations of the International Union of Geological Sciences Subcommission on the Systematics of Metamorphic Rocks: University Press Cambridge, Cambridge, pp. 93-110.

Sorensen, S., Harlow, G.E., Rumble, D., 2006. The origin of jadeitite-forming subduction-zone fluids: CL-guided SIMS oxygen-isotope and trace-element evidence. American Mineralogist 91, 979-996.

Sun, S. S., McDonough, W.F., 1989. Chemical and isotopic systematics of oceanic basalts: implications for mantle composition and processes. In: Saunders, A.D., Norry, M.J.

(Eds.), Magmatism in the ocean basins: Geological Society London Special Publications, 42, pp. 313-345.

Tsuchiyama, A., Takahashi, E., 1983. Melting kinetics of a plagioclase feldspar. Contributions to Mineralogy and Petrology 84, 345-354.

von Blanckenburg, F., Davies, J.H., 1995. Slab breakoff: A model for syncollisional magmatism and tectonics in the Alps. Tectonics 14, 120-131.

Whalen, J.B., McNicoll, V.J., van Staal, C.R., Lissenberg, C.J., Longstaffe, F.J., Jenner, G.A., van Breeman, O., 2006. Spatial, temporal and geochemical characteristics of Silurian collision-zone magmatism, Newfoundland Appalachians: An example of a rapidly evolving magmatic system related to slab break-off. Lithos 89, 377-404.

Whitney, D.L., 2002. Coexisting andalusite, kyanite, and sillimanite: Sequential formation of three Al_2SiO_5 polymorphs during progressive metamorphism near the triple point, Sivrihisar, Turkey. American Mineralogist 87, 405-416.

Whitney, D.L., Davis, P.B., 2006. Why is lawsonite eclogite so rare? Metamorphism and preservation of lawsonite eclogite, Sivrihisar, Turkey. Geology 34, 473-476.

Whitney, D., Teyssier, C., Toraman, E., Seaton, N., Fayon, A., 2011. Metamorphic and tectonic evolution of a structurally continuous blueschist-to-Barrovian terrane, Sivrihisar Massif, Turkey. Journal of Metamorphic Geology 29, 193-212.

Wilson, M., 1989. Igneous petrogenesis. Unwin Hyman, Boston.

Table 1. Previously reported ages of metamorphic minerals from the Tavşanlı Zone assemblages (excluding the Sivrihisar Massif).

Age (Ma)	Reference[a]	Age (Ma)	Reference
		$^{40}Ar/^{39}Ar$ phengite[b]	
192±8 to 92±11	S(1999)	89.3±0.7	OK(1994)
123±7 to 93±3	SK(2002)	89±1 to 75±6	S(1999); SK(2002)
118±3 to 102±4	S(1999)	86.7±0.7	OK(1994)
111±3 to 86±3	S(1999)	86.5±1.2 to 85.9±1.2	S(1999)
110±3 to 94±2	S(1999)	83.5±1.6	OK(1994)
108±3 to 90±4	SK(2002)	81.4±10.2	OK(1994)
104±9 to 91±15	SK(2002)	71.5±0.7	OK(1994)
		70.7±1.2	OK(1994)
$^{40}Ar/^{39}Ar$ glaucophane or amphibole		K-Ar muscovite	
130±6	SK(2002)	156±3	CK(1967)
118±2	S(1999)	82±2	CK(1967)
108.1±3.7	H(1994)	65±2	CK(1967)
101.1±3.8	H(1994)		
Rb-Sr		$^{40}Ar/^{39}Ar$ lawsonite	
79.7±1.6	S(1999)	216±30 to 117±17	SK(2002)
78.5±1.6	S(1999)		

[a] Reference abbreviations: Cogulu and Krummenacher (1967)= CK(1967); Harris et al. (1994)= H(1994); Okay and Kelly (1994)= OK(1994); Sherlock and Kelley (2002)= SK(2002); Sherlock et al. (1999)=S(1999).

[b] Range represents ages from a single sample.

Table 2. Previously reported ages of metamorphic minerals from the Sivirhisar Massif.

Age (Ma)	Reference[a]	Age (Ma)	Reference
		$^{40}Ar/^{39}Ar$ phengite[b]	
168±49 to 84±2	SK(2002)	105±5 to 86±4	S(1999)
112±4 to 82±2	SK(2002)	105±2 to 78±2	S(1999)
111±11 to 78±2	SK(2002)	100±5 to 72±3	SK(2002)
109±3 to 78±2	SK(2002)	89±5 to 78±4	SK(2002)
107±3 to 72±3	S(1999)	87.9±0.3	S(2009)
107±3 to 83±2	SK(2002)	85±5 to 79±4	SK(2002)
	$^{40}Ar/^{39}Ar$ glaucophane		Rb-Sr
154±3	S(1999)	82.8±1.7	S(1999)
109±7	SK(2002)	80.1±1.6	S(1999)
	$^{40}Ar/^{39}Ar$ muscovite		
60.4±0.1	S(2009)		
58.8±0.1	S(2009)		

[a] Reference abbreviations: Seaton et al. (2009)= S(2009); Sherlock and Kelley (2002)= SK(2002); Sherlock et al. (1999)=S(1999);

[b] Range represents ages from a single sample.

Table 3. Previously reported ages of minerals from Sivrihisar and Kaymaz granitoids.

Age (Ma)	Method	Reference
	Sivrihisar Pluton	
90.82±2.14	U-Pb zircon	Gautier (1984)
71±3	K-Ar hornblende	Cogulu and Krummenacher (1967)
62.9±1.3	K-Ar biotite	Delaloye and Bingöl (2000)
61.0±1.4	K-Ar feldspar	Delaloye and Bingöl (2000)
56.8±1.2	K-Ar hornblende	Delaloye and Bingöl (2000)
53.0±3.0	$^{40}Ar/^{39}Ar$ hornblende	Sherlock et al. (1999)
48.95±4.49	U-Pb apatite	Gautier (1984)
	Kaymaz Pluton	
84.98±6.27	U-Pb zircon	Gautier (1984)

Table 4. Sample locations and assemblages.

Sample[a]	Location		Mineral Assemblage[b]
		Sivrihisar Pluton	
TA04	39°26'06.10" N	31°32'22.70"E	Qtz+Pl+Hbl+Kfs+Ms+Bt+Opx+Ttn +Zr+Ap+Opq+Aln
TA04A	-	-	Qtz+Pl+Hbl+Kfs+Ms+Bt+Opx+Zr+Ap+Opq
TA04A-1			Qtz+Pl+Hbl+Kfs+Ms+Bt+Opx+Zr+Ap+Opq
TA04A-2			Qtz+Pl+Hbl+Kfs+Ms+Bt+Opx+Zr+Ap+Opq
TA04B	-	-	Qtz+Pl+Hbl+Kfs+Ms+Bt+Opx+Zr+Ap+Opq+ Ttn+Ilm
		Kaymaz Pluton	
TA05A	39°30'14.50" N	31°15'06.00"E	Pl+Qtz+Ser+Ms+Opq+Zr+Thr+Mnz+Ilm+Rt+ Brt+Py+Cal
TA05B	39°30'12.60" N	31°15'14.40"E	Pl+Qtz+Ser+Opq+Zr+Cal+Brt+Chr
		Mica Schist	
TA02A	39°28'03.80" N	31°37'49.50"E	Qtz+ Ms+Phg+ Chl +Stp+Ilm+Zr+Mnz+Opq

[a] See Figure 2 for locations. The "A" or "B" nomenclature refers to multiple samples collected from the same location.

[b] Mineral abbreviations after Siivola and Schmid (2007).

Table 5. Major element concentrations (wt%) from Sivrihisar and Kaymaz plutons.

Element [a]	TA04A-1[b]	TA04A-2[b]	TA05A[c]	TA05B[c]
SiO_2	64.29	58.50	81.99	96.43
Al_2O_3	17.37	17.83	11.72	0.45
Fe_2O_3[d]	2.83	5.27	0.89	0.90
MnO	0.038	0.117	0.005	0.008
MgO	0.72	2.12	0.07	0.23
CaO	2.40	5.75	0.07	0.12
Na_2O	3.69	4.47	0.02	0.04
K_2O	7.64	3.45	0.29	0.05
TiO_2	0.315	0.514	0.100	0.006
P_2O_5	0.16	0.33	0.02	0.01
LOI[e]	0.39	1.61	4.34	0.95
Total	99.83	99.97	99.51	99.2
MALI[f]	8.93	2.17	0.24	-0.03
FM[g]	0.797	0.713	0.927	0.796
ASI[h]	0.938	0.843	26.0	1.380

[a] All elements were obtained using Fusion Inductively Coupled Plasma Spectrometry. Detection limit for all elements is 0.01 wt% with the exception of MnO and TiO_2 (0.001%). See Figure 2 for sample locations.

[b] Sivrihisar sample. The "-1" and "-2" nomenclature refers to chips 1 and 2 respectively.

[c] Kaymaz sample.

[d] Fe_2O_3 is measured total.

[e] LOI = Loss on Ignition.

[f] MALI= Modified Alkaline Lime Index ($Na_2O + K_2O – CaO$); see Frost et al. (2001).

[g]FM= Fe_2O_3/(Fe_2O_3 +MgO); see Frost et al. (2001).

[h]ASI= Aluminosaturation Index (ASI; Al/Ca-1.67P+Na+K); see Frost et al. (2001).

Table 6. Trace element concentrations (ppm) from the Sivrihisar and Kaymaz plutons.[a]

Element[a]	TA04 A-1[b]	TA04 A-2[b]	TA05A[c]	TA05B[c]	Element	TA04 A-1[b]	TA04 A-2[b]	TA05A[c]	TA05B[c]
Sc	6	10	<1	<1	Sn	11	3	8	3
Be	8	3	2	<1	Sb	<0.5	<0.5	38.3	62.5
V	44	114	7	11	Cs	2.8	1.4	3.4	1.1
Ba	1444	1509	26	832	La	151	68.4	30.2	1.2
Sr	1598	1533	76	38	Ce	251	123	41.7	2
Y	22	21	3	<2	Pr	26.3	14.7	3.3	0.19
Zr	467	187	86	5	Nd	82.6	52.4	8.0	0.6
Cr	<20	70	140	2020	Sm	12.7	9.0	0.9	<0.1
Co	3	17	1	9	Eu	2.8	2.2	0.14	<0.05
Ni	<20	<20	<20	100	Gd	7.3	5.9	0.6	<0.1
Cu	180	40	<10	<10	Tb	0.9	0.8	<0.1	<0.1
Zn	40	60	60	30	Dy	4.4	4.1	0.5	<0.1
Ga	23	21	15	<1	Ho	0.7	0.7	0.1	<0.1
Ge	1	1	1	1	Er	1.9	2.0	0.3	<0.1
As	<5	<5	162	94	Tm	0.26	0.29	0.07	<0.05
Rb	196	82	16	2	Yb	1.6	1.9	0.5	<0.1
Nb	32	12	27	<1	Lu	0.25	0.29	0.08	<0.04
Mo	<2	<2	15	<2	Hf	12.8	4.7	3.0	<0.2
Ag	1.3	<0.5	<0.5	4.4	Ta	3.5	0.9	2.2	<0.1
Bi	<0.4	<0.4	5	1	W	<1	<1	18	1

Th	98.7	12.5	51.9	0.9	Tl	1.1	0.4	0.2	0.5
U	14.0	4.8	11.1	0.9	Pb	106	32	196	<5

[a] All elements reported as parts per million (ppm). See Figure 2 for sample locations. In was measured but not detected (<0.2 ppm).

[b] Sivrihisar sample. The "-1" and "-2" nomenclature refers to chips 1 and 2 respectively.

[c] Kaymaz sample.

Table 7. Geochronologic results.

zirc_ spot[a]	$^{238}U/^{206}Pb$[b] Age (Ma) (±1σ)[b]	$^{238}U/^{206}Pb$ Age (Ma) (±1σ)[c]	$^{235}U/^{207}Pb$ Age (Ma) (±1σ)[b]	$^{235}U/^{207}Pb$ Age (Ma) (±1σ)[c]	% $^{206}Pb^*$ (±1σ)[d]	% $^{206}Pb^*$ (±1σ)[e]	UO^+/U^+ (±1σ)[f]
Sivrihisar Granite: TA04							
z2s1	78.4 (8.5)	79.9 (8.6)	74.8 (22.2)	99.8 (14.9)	88.0 (1.5)	89.7 (0.7)	7.240 (0.029)
z4s1	64.9 (6.4)	64.0 (5.6)	NAN[g]	NAN	71.5 (4.8)	70.6 (2.0)	7.688 (0.071)
z3s1	48.9 (4.5)	49.8 (4.6)	42.1 (11.1)	57.6 (7.8)	93.9 (1.2)	95.7 (0.6)	7.494 (0.033)
z1s1	44.8 (2.6)	46.2 (2.5)	NAN	45.2 (10.7)	78.6 (2.8)	81.1 (1.1)	8.989 (0.058)
z5s1	41.9 (2.3)	42.4 (2.3)	36.5 (4.9)	44.6 (3.5)	98.2 (0.6)	99.3 (0.3)	8.673 (0.042)
Sivrihisar Granite: TA04B							
z2s1	70.1 (6.7)	58.8 (4.5)	245.5 (72.2)	NAN	43.4 (6.9)	36.4 (3.7)	8.202 (0.085)
Kaymaz Granite: TA05A							
z6s1	42.5 (2.2)	39.9 (2.1)	NAN	NAN	17.7 (2.5)	16.6 (2.4)	9.203 (0.019)
z8s1	41.6 (4.5)	44.3 (4.9)	NAN	NAN	6.0 (9.3)	6.4 (9.4)	11.00 (0.07)
z7s1	40.7 (1.7)	41.2 (1.7)	50.2 (10.3)	58.9 (9.4)	71.7 (1.2)	72.6 (1.0)	9.553 (0.026)
z4s1	39.7 (4.7)	19.4 (4.5)	155.5 (72.4)	NAN	3.2 (10.9)	1.6 (22.7)	9.075 (0.021)
z2s1	33.3 (2.0)	33.3 (1.8)	71.5 (23.4)	71.6 (20.4)	15.4 (3.4)	15.4 (2.8)	9.585 (0.023)
Mica Schist: TA02A							
z4s2	1859 (102)	1870 (102)	1859 (54)	1902 (55)	99.95 (0.02)	100.7 (0.1)	8.307 (0.054)
z4s1	1628 (81)	1646 (81)	1736 (47)	1809 (48)	99.94 (0.02)	101.2 (0.2)	8.545 (0.036)
z3s1	562 (32)	564.8 (32.1)	580 (30)	615 (33)	98.0 (0.2)	95.8 (0.3)	8.416 (0.024)
z3s2	307 (16)	310.8 (16.0)	350 (19)	395 (18)	99.2 (0.2)	100.3 (0.1)	8.756 (0.053)

z2s1	116 (9)	116 (9)	138 (22)	138 (14)	89.3 (1.0)	89.3 (0.5)	7.909 (0.032)
z1s1	87.0 (5.5)	87.8 (5.6)	76 (7)	89 (6)	93.2 (0.4)	94.1 (0.1)	8.209 (0.019)
z1s2	82.3 (7.1)	86.9 (7.2)	16.8 (42)	95 (16)	71.6 (2.8)	75.6 (0.8)	7.725 (0.054)

[a] Nomenclature refers to grain number (z#) and ion microprobe spot number (s#).

[b] Ages calculated using a common ^{204}Pb correction where ^{204}Pb was measured in the sample.

[c] Age calculated using the ^{208}Pb correction assuming ^{206}Pb/^{204}Pb=18.86, ^{207}Pb/^{204}Pb=15.62, and ^{208}Pb/^{204}Pb=38.34.

[d] Percent radiogenic ^{206}Pb if using the ^{204}Pb correction

[e] Percent radiogenic ^{206}Pb if using the ^{208}Pb correction

[f] Ideally the UO^+/U^+ of the sample lies within the range of the calibration curve, which is 8.561±0.029 to 7.028±0.014.

[g] NAN= result not meaningful as errors are too large (±1σ is >50% of absolute age).

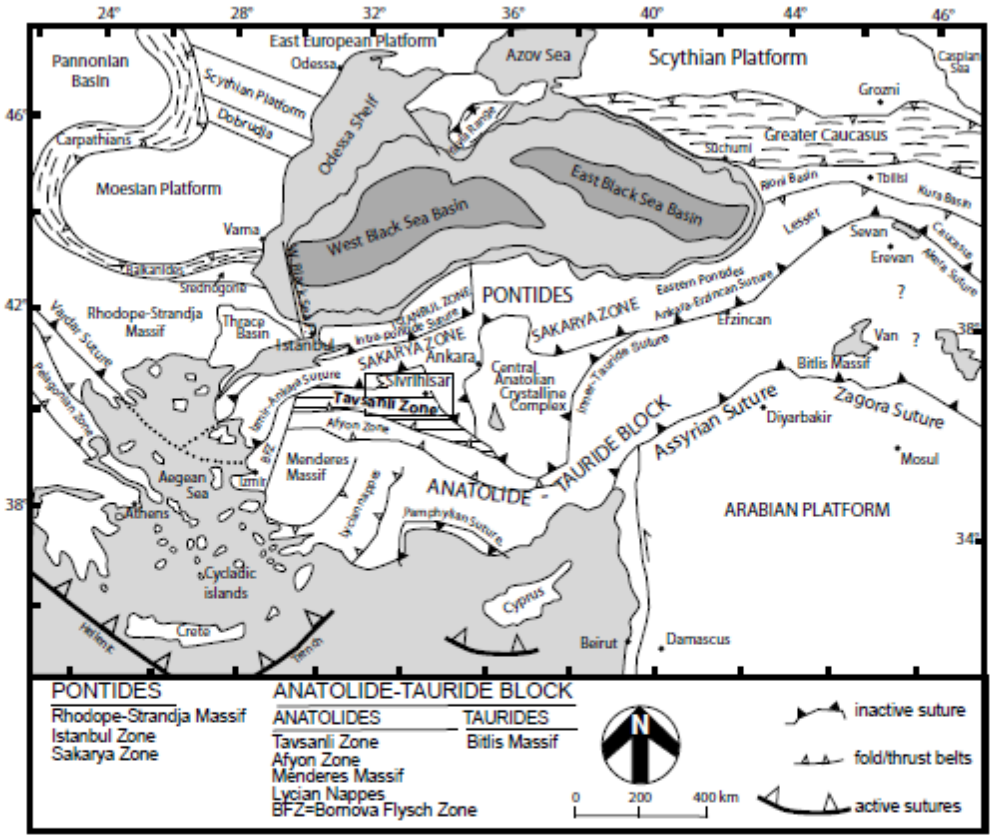

Shin et al. Figure 1

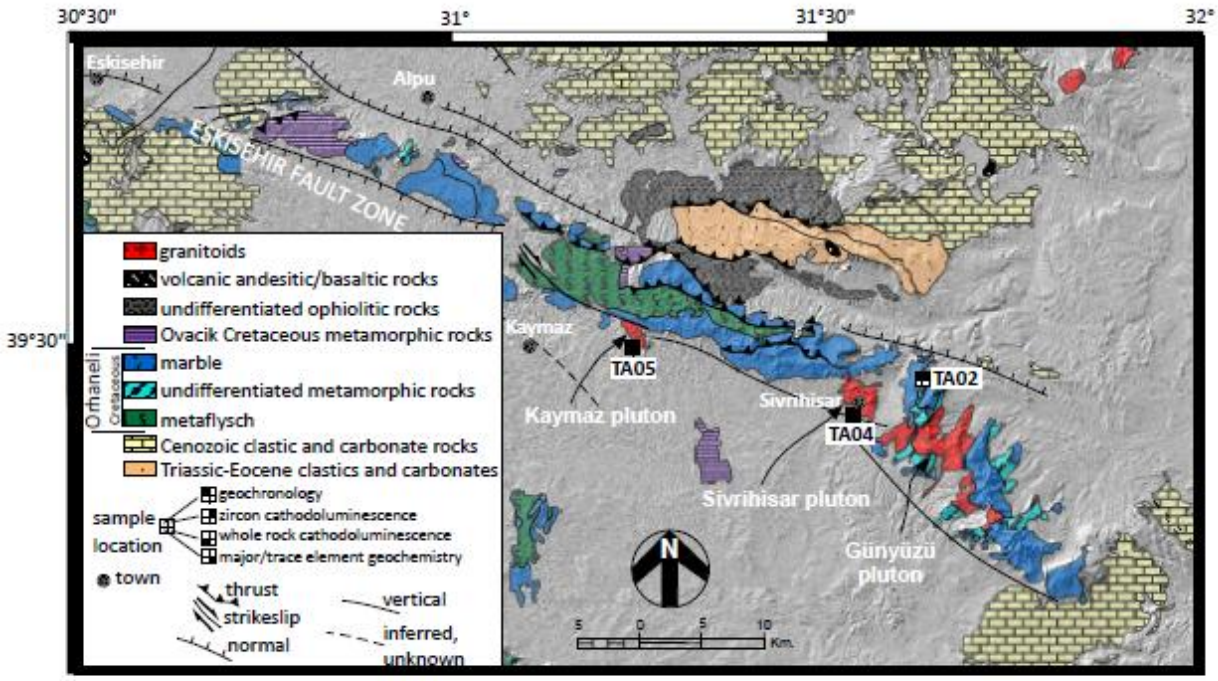

Shin et al. Figure 2

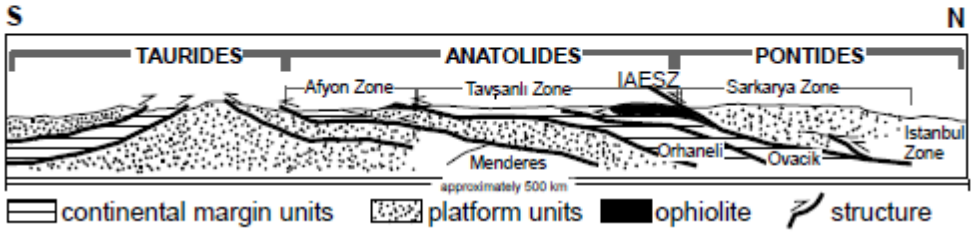

Shin et al. Figure 3

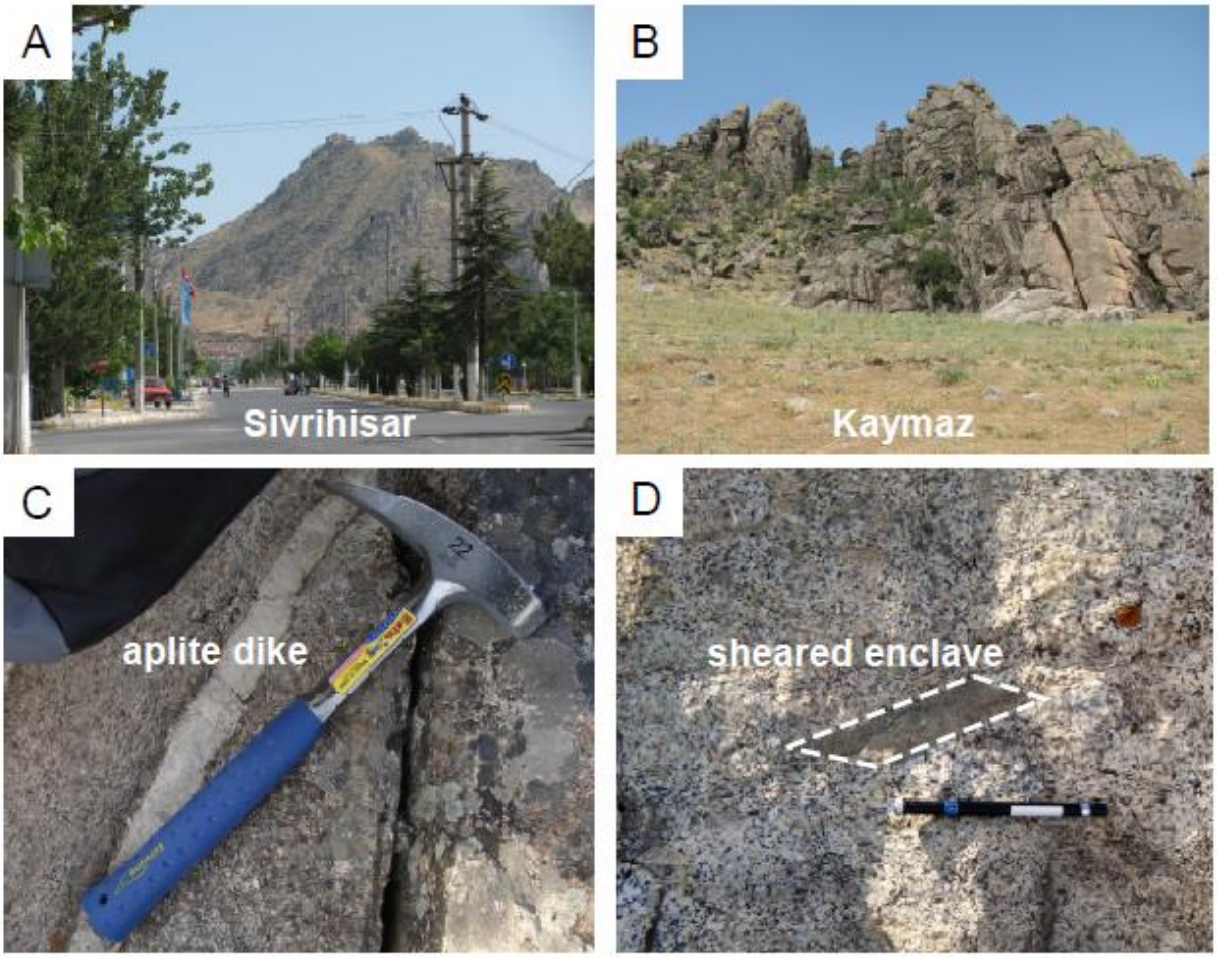

Shin et al. Figure 4

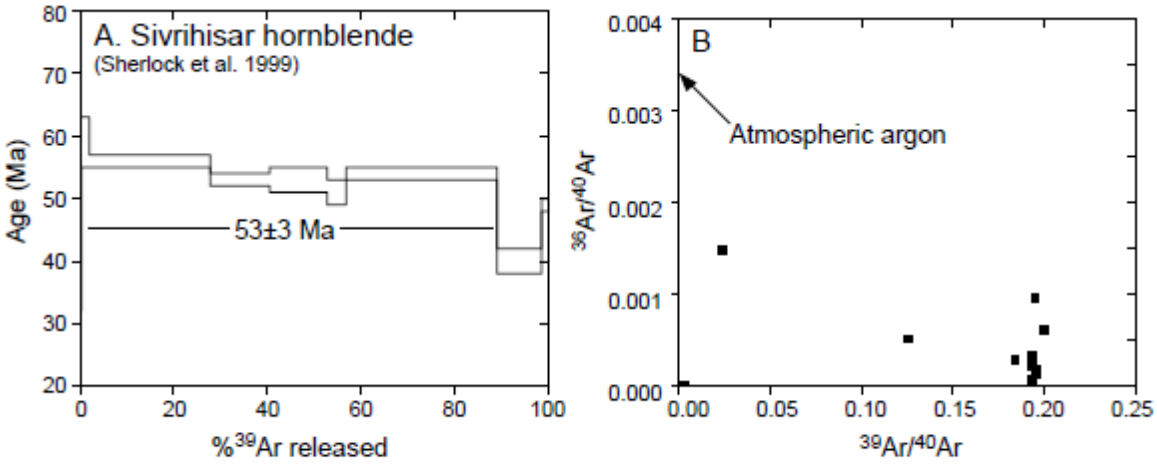

Shin et al. Figure 5

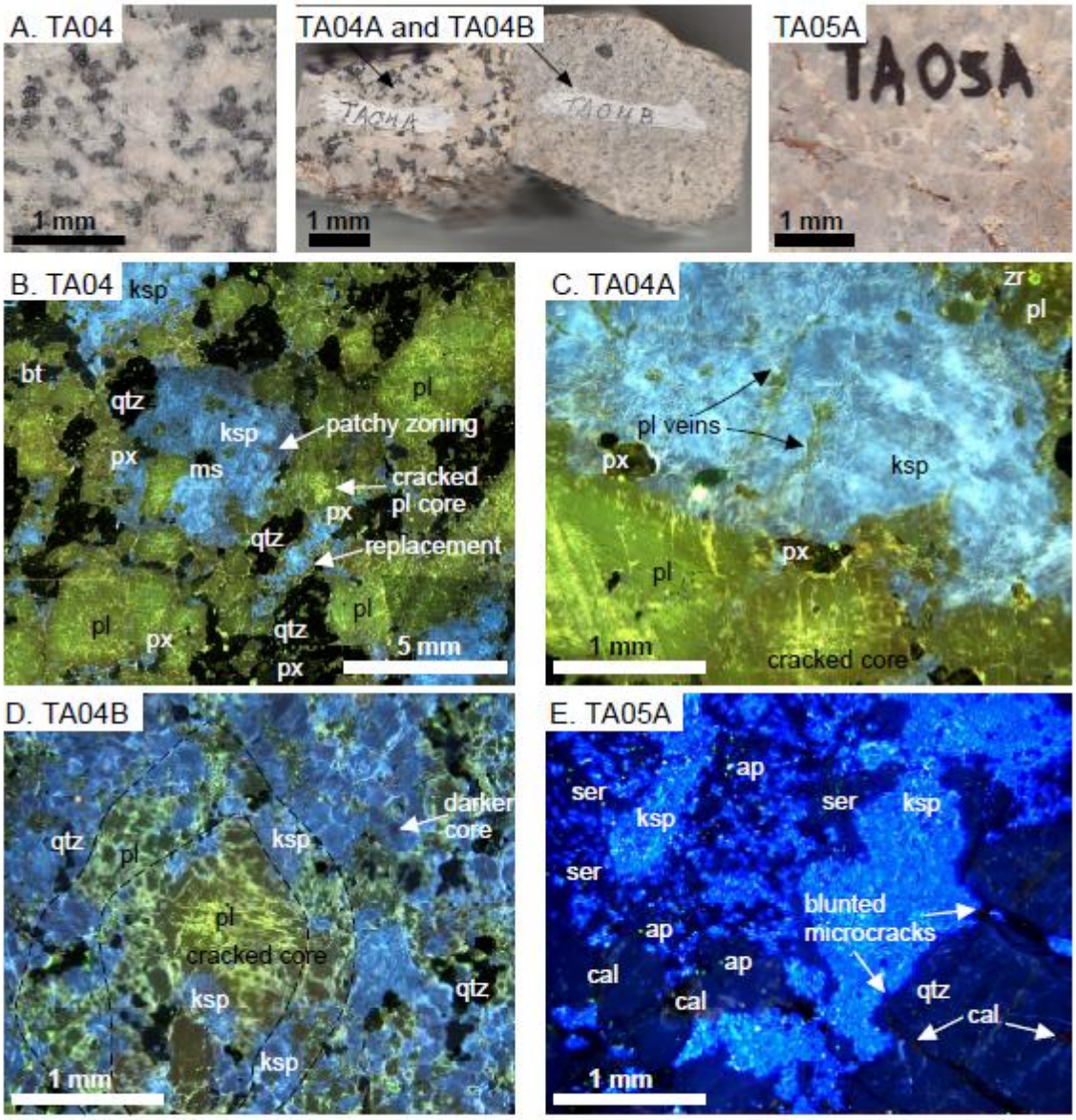

Shin et al. Figure 6

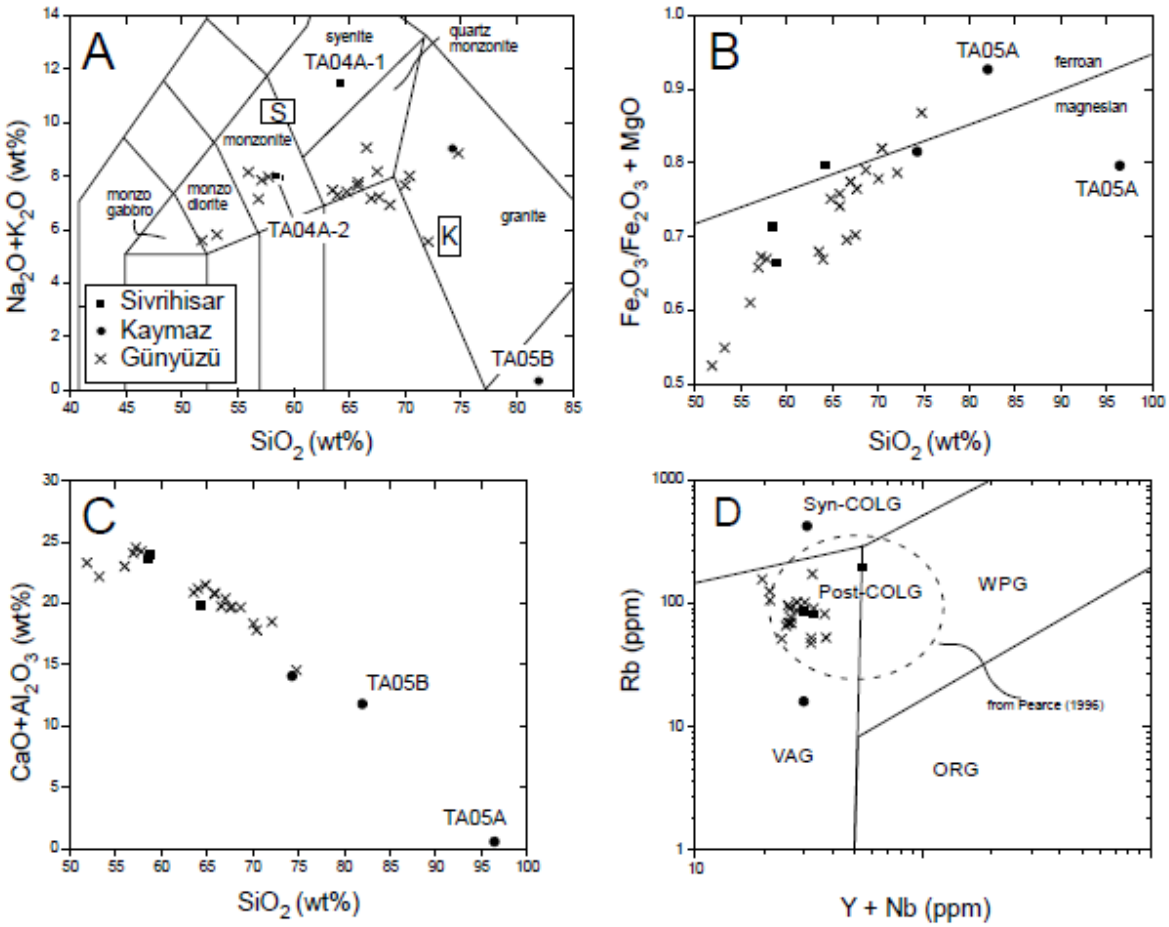

Shin et al. Figure 7

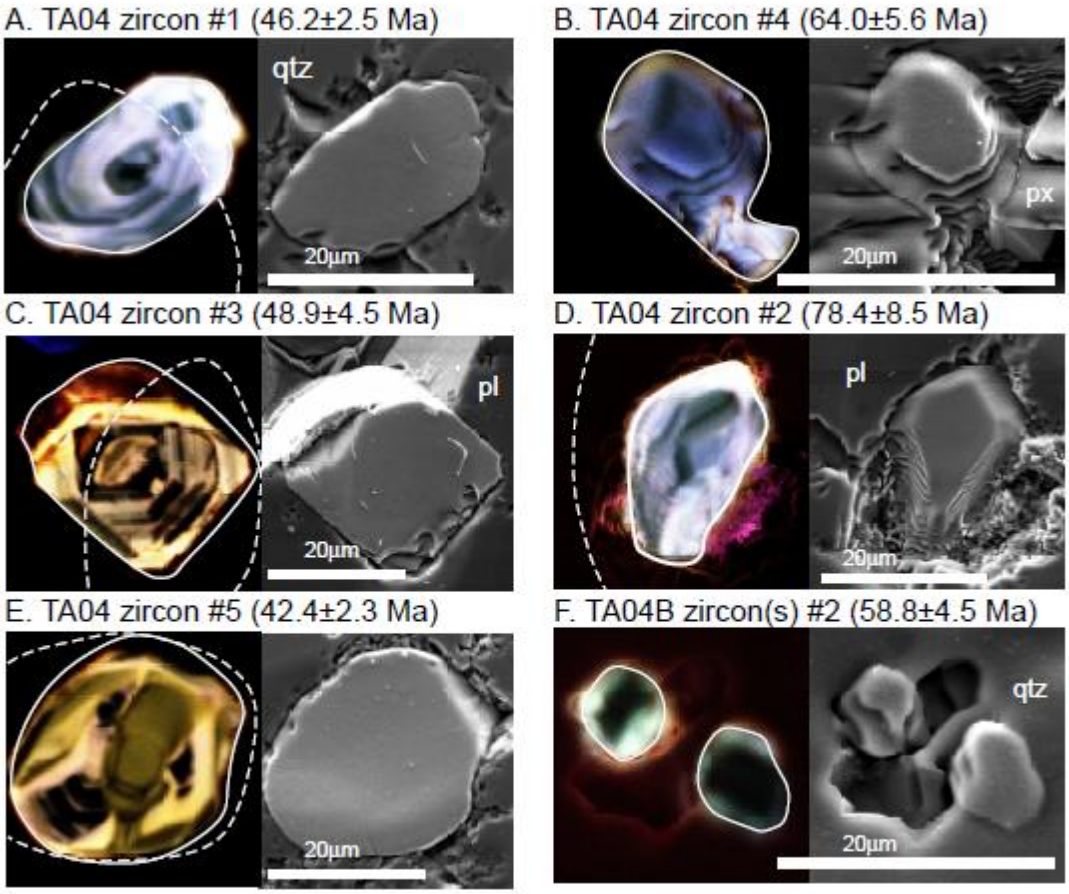

Shin et al. Figure 8

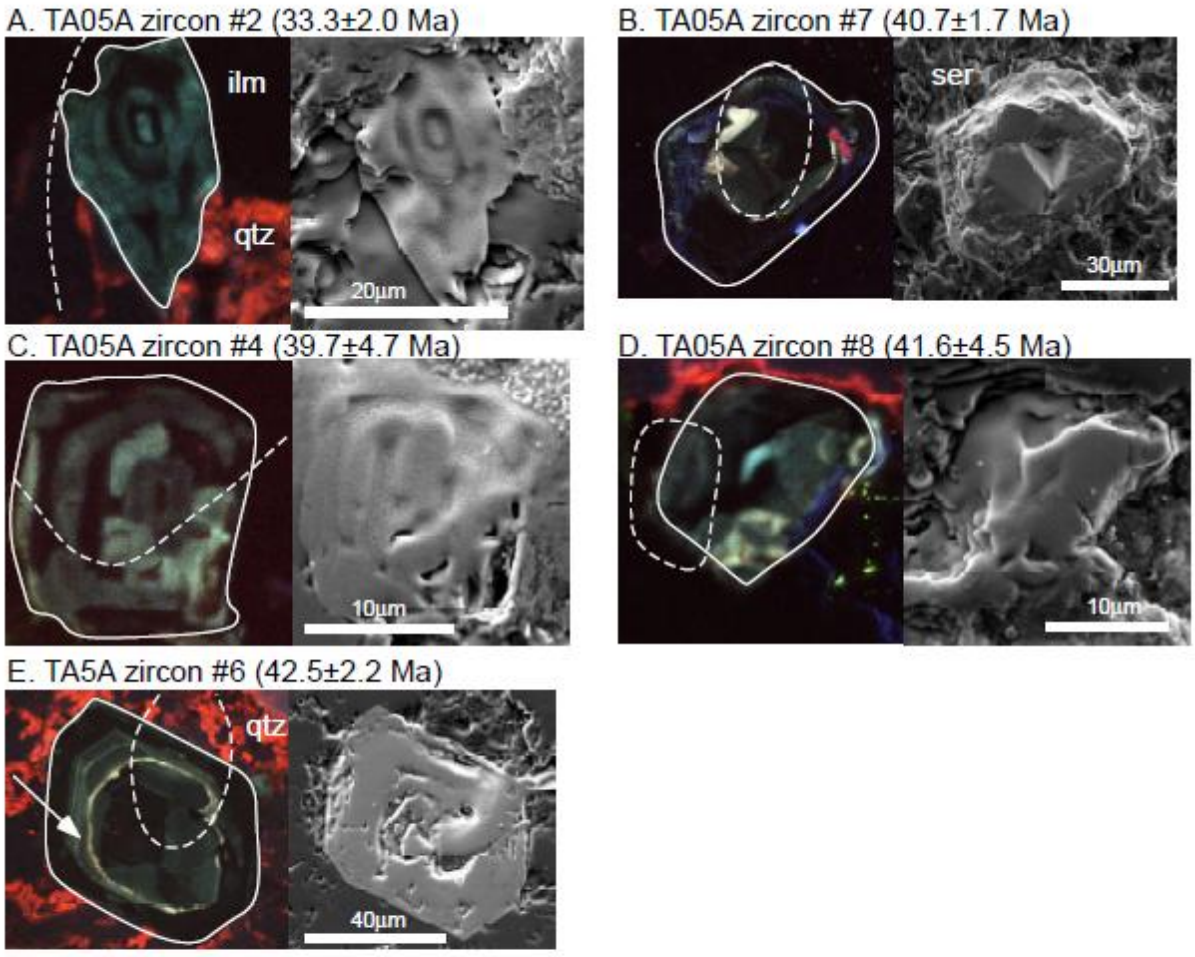

Shin et al. Figure 9

A. TA02A zircon #3
spot 1: 562±32 Ma; spot 2: 307±16 Ma

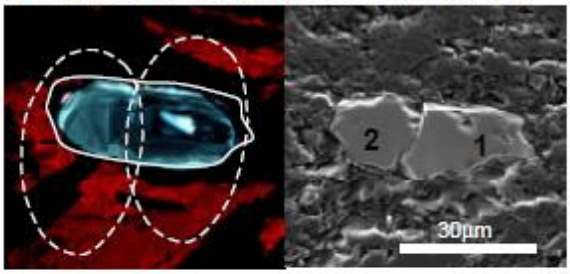

B. TA02A zircon #2 (116±8 Ma)

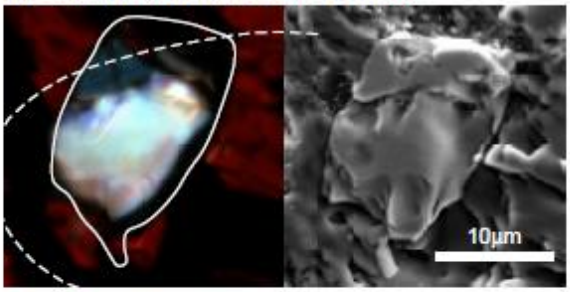

C. TA02A zircon #1
spot 1: 87.8±5.6 Ma; spot 2: 86.9±7.2 Ma

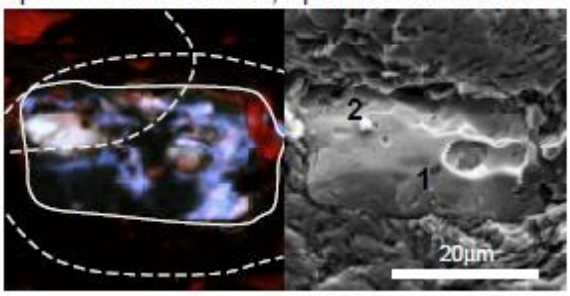

D. TA02A zircon #4
spot 1: 1628±81 Ma; spot 2: 1859±102 Ma

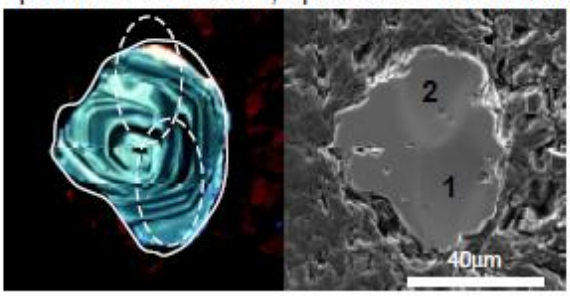

Figure 10

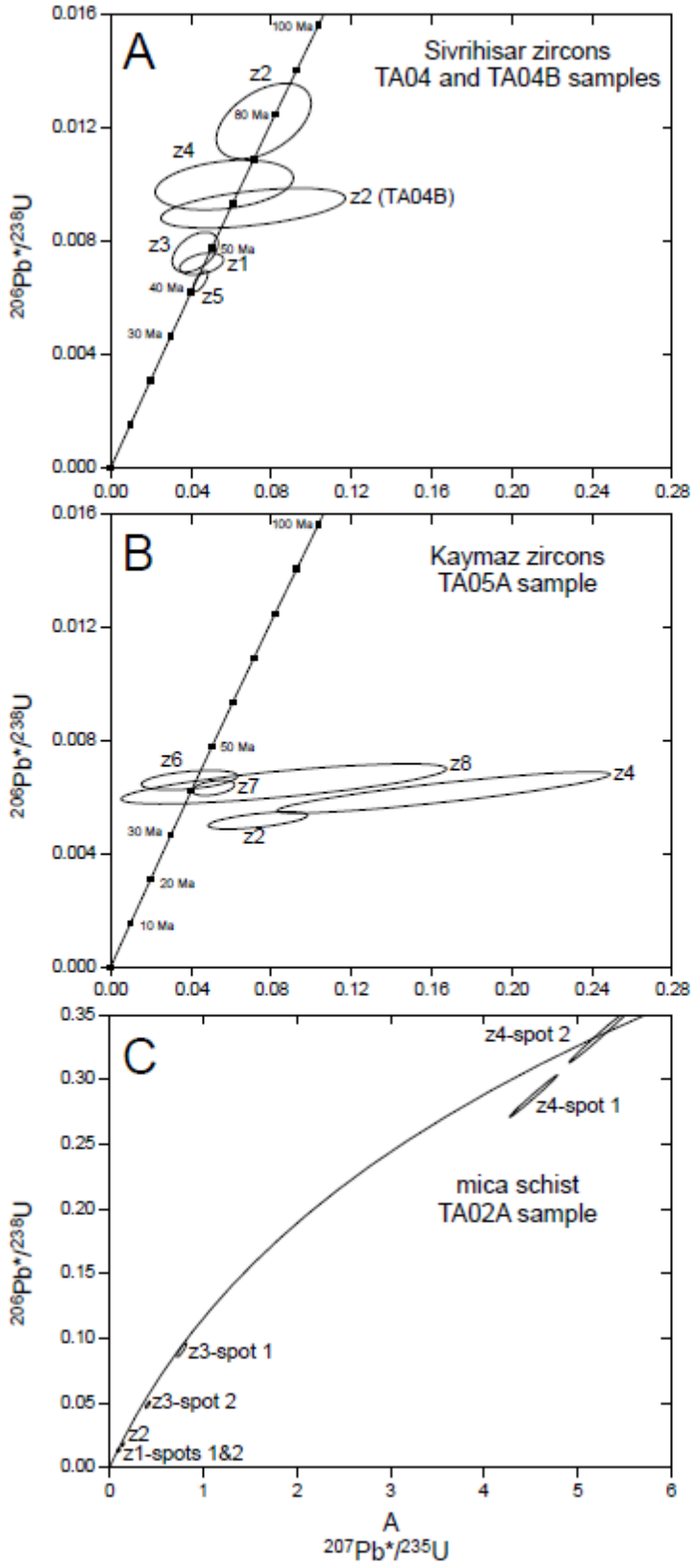

Shin et al.
Figure 11

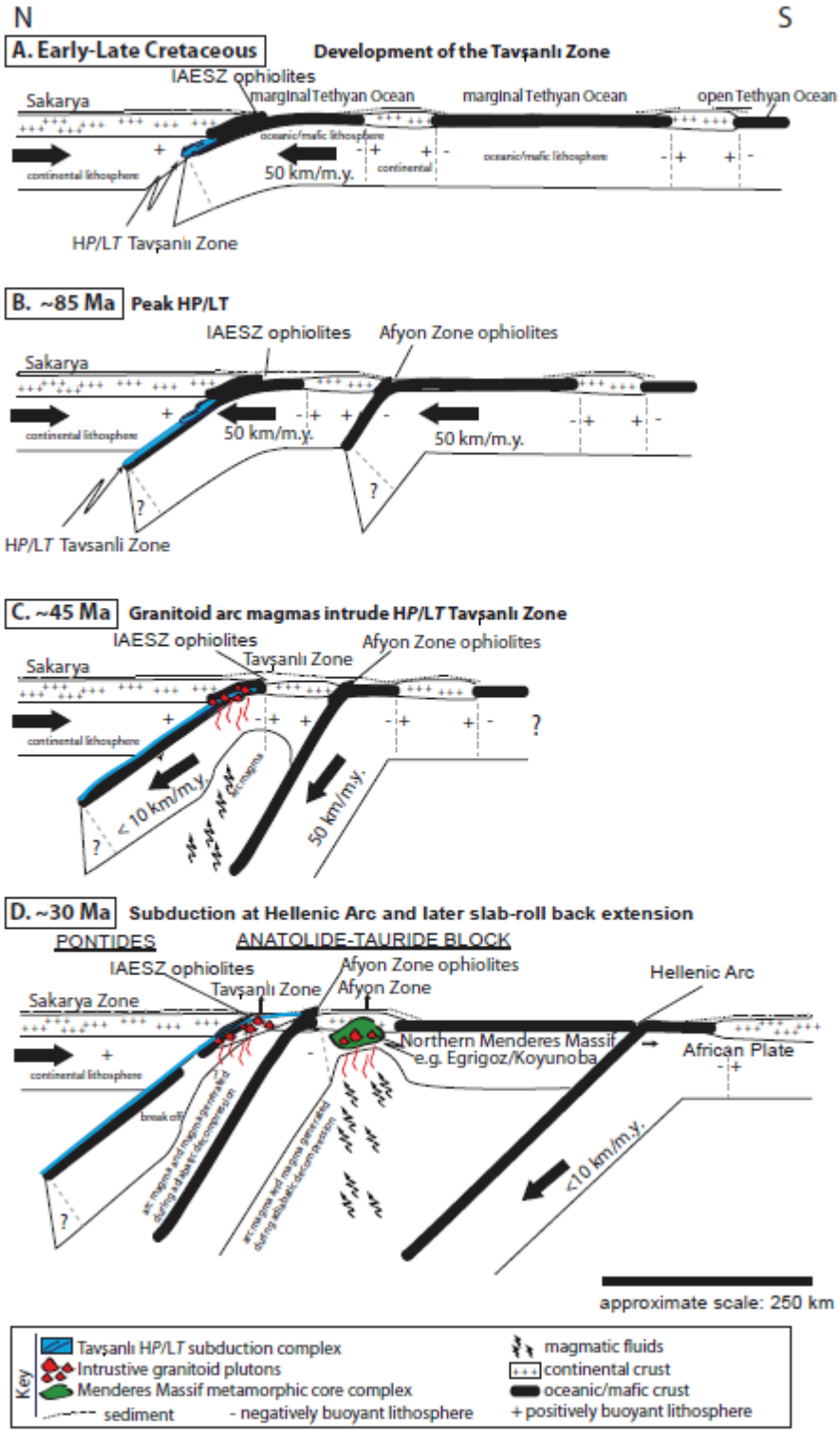

Shin et al. Figure 12

Research Highlights

- Granitoids from the Sivrihisar Massif in Tavşanlı Zone record zircon ages from the Late Cretaceous to the Oligocene.
- Granites show complex textures and geochemistry, and may be sourced from a subduction zone located ~200 km to the south.
- CL images of granites from this region show evidence for fluid interactions at the subsolidus and lower temperature stages.
- Subduction along the Tavşanlı Zone was ongoing during the Late Cretaceous but entrained zircons with igneous zoning that crystallized during the Paleoproterozoic, Cambrian, and Carboniferous.
- Presents a model in which the Tavşanlı Zone is the northernmost segment of an amalgamation of stacked subduction zones that progressively transition from north to south over time.